

# Multiparametric high-resolution imaging of native proteins by force-distance curve-based AFM

Moritz Pfreundschuh<sup>1</sup>, David Martinez-Martin<sup>1</sup>, Estefania Mulvihill<sup>1</sup>, Susanne Wegmann<sup>2</sup> & Daniel J Muller<sup>1</sup>

<sup>1</sup>Department of Biosystems Science and Engineering, ETH Zurich, Basel, Switzerland. <sup>2</sup>Department of Neurology, Massachusetts General Hospital, Harvard Medical School, Charlestown, Massachusetts, USA. Correspondence should be addressed to D.J.M. (daniel.mueller@bsse.ethz.ch).

Published online 17 April 2014; doi:10.1038/nprot.2014.070

**A current challenge in the life sciences is to understand how the properties of individual molecular machines adjust in order to meet the functional requirements of the cell. Recent developments in force-distance (FD) curve-based atomic force microscopy (FD-based AFM) enable researchers to combine sub-nanometer imaging with quantitative mapping of physical, chemical and biological properties. Here we present a protocol to apply FD-based AFM to the multiparametric imaging of native proteins under physiological conditions. We describe procedures for experimental FD-based AFM setup, high-resolution imaging of proteins in the native unperturbed state with simultaneous quantitative mapping of multiple parameters, and data interpretation and analysis. The protocol, which can be completed in 1–3 d, enables researchers to image proteins and protein complexes in the native unperturbed state and to simultaneously map their biophysical and biochemical properties at sub-nanometer resolution.**

## INTRODUCTION

Proteins, lipids, nucleic acids and other biomolecules form the highly sophisticated molecular machinery of the living cell that works and responds to its environment in a complex manner. To fulfill their versatile functions, these molecular machines have heterogeneous structural, biophysical and biochemical properties that can change dynamically as required by the cell. Atomistic and theoretical models are frequently applied to calculate these properties<sup>1–6</sup>; however, such calculated properties can be quite different from those determined experimentally. The reasons for such discrepancies can be manifold. For instance, the biophysical and biochemical properties of molecular machines change depending on pH, electrolyte concentration, temperature and interactions with other biomolecules.

As intracellular conditions are highly heterogeneous, the properties of molecular machines depend on the machines' location within the cell. In addition, the structural and functional properties of most molecular machines vary between individuals. Therefore, conventional bulk methods, such as those applied to determine structural (e.g., X-ray or electron crystallography, NMR, circular dichroism spectroscopy) or functional details (e.g., enzymatic assays, calorimetry, UV-visible spectroscopy), mostly provide information on the prevailing conditions of molecular machines. It is important to quantify and structurally map the biophysical and biochemical properties of single molecular machines in the living cell or at least in physiologically relevant conditions<sup>7–10</sup>.

Single-molecule approaches enable researchers to address the individuality of the cellular machinery and the role of heterogeneity. Recent developments in FD curve-based AFM enable one to combine sub-molecular imaging with quantitative mapping of physical, chemical and biological properties<sup>11,12</sup>. In the following sections, we provide a brief overview of the history of high-resolution (~1 nm) AFM imaging and AFM-based force spectroscopy of native proteins. We discuss how, at present, both applications are combined in FD-based AFM, which enables the quantitative multiparametric imaging and characterization of biomolecular systems under physiological conditions. Finally, we present protocols for applying FD-based AFM to the

characterization of native proteins and protein complexes *in vitro*. Although the protocols are applied to the quantitative imaging of native membrane and water-soluble proteins, they are equally applicable to imaging nucleic acids, whether as single molecules or in complex, as well as to other biomolecules that shape the molecular machinery of the cell.

## High-resolution AFM imaging of single native proteins

AFM was originally conceived as a tool for the high-resolution imaging of the surface of objects in air, under vacuum and, most importantly for biological applications, in buffered solution<sup>13–15</sup>. Thus, it is straightforward to apply AFM to the imaging of native biological specimens<sup>16</sup>. In its early years, AFM was operated mainly in contact mode, in which the AFM stylus is pressed onto the sample with constant force while it is 'contouring' the sample surface (imaging the surface of the sample by measuring contact interaction). Contact-mode AFM applied to smooth biological samples, such as membrane proteins embedded in their native lipid bilayer, revealed surprising structural details<sup>17–21</sup>. Atomistic structural models assessing AFM topographs have shown that contact-mode imaging, if properly adjusted, enables to contour the surface of native proteins at sub-nanometer resolution<sup>18,22</sup>. The best attainable lateral and vertical resolutions of native membrane proteins approach 0.5–0.7 nm and ~0.1 nm, respectively<sup>23,24</sup>.

In addition to achieving such high resolutions, time-lapse AFM enabled the observation of single membrane proteins at work<sup>25,26</sup>. Examples include the surface layer (S-layer) from *Deinococcus radiodurans*<sup>27</sup>, the outer membrane proteins (Omps) OmpG and OmpF from *Escherichia coli*<sup>24,28</sup>, the connexins that form communication channels of epithelial cells<sup>29,30</sup>, the light-driven proton pump bacteriorhodopsin from *Halobacterium salinarum*<sup>31,32</sup>, the ATP-gated P2X<sub>4</sub> purinergic receptor<sup>33</sup>, the ligand-gated potassium channel MlotiK1 from *Mesorhizobium loti*<sup>34</sup> and the pH-gated KcsA potassium channel<sup>35</sup>. Membrane proteins have also been imaged in motion during diffusion, assembly and rotation<sup>36–42</sup>.

A disadvantage of AFM imaging in contact mode is that lateral forces between the scanning AFM stylus and the soft

## PROTOCOL

biological sample are difficult to control. Consequently, single proteins, fibrils or larger complexes that show corrugations of more than a few nanometers in height are easily deformed or displaced from their support by the scanning AFM stylus. To address this problem, oscillation-mode AFM, in which the AFM stylus oscillates vertically and interacts with the fragile biological sample at the end of the downward movement, was introduced<sup>43–45</sup>. Interaction with the sample changes the amplitude (or frequency) of the oscillating AFM stylus, which is used as feedback to contour the sample. This approach markedly reduces the contact time and friction between the AFM stylus and the sample and enables you to image weakly adsorbed biomacromolecules that are difficult to image using contact-mode AFM<sup>46–57</sup>.

As applied to membrane proteins, the smallest structural details observed using oscillation-mode AFM approach in size those observed using contact-mode AFM<sup>58</sup>. However, the mechanisms that contribute to the contrast of oscillation-mode AFM images in liquids are not well understood, which sometimes makes the data collected difficult to interpret<sup>59–63</sup>. Because, compared with contact-mode AFM, oscillation-mode AFM is so much easier to use and often less invasive, it is widely used for the imaging of biological samples. Consequently, a broad range of native proteins can be observed at work by using oscillation-mode AFM<sup>31,51,56,64–66</sup>. A shortcoming of both contact- and oscillation-mode AFM is that they are limited in terms of quantifying and mapping biological, chemical and physical parameters. In the following section, we discuss the use of AFM in force-spectroscopy mode, which enables the quantification of the manifold interactions occurring between the AFM stylus and the biological sample under physiologically relevant conditions.

### Force spectroscopy of single proteins

Shortly after the first applications of AFM to image biological systems, it was observed that the AFM stylus can be used for micro- and nanomanipulation. Early AFM-based manipulations included the dissection of nucleic acids, membrane protein complexes, junctional membranes and chromosomes<sup>36,67–69</sup>. It was also observed that the AFM stylus can act as a nanometer-sized probe and quantify electrostatic, van der Waals and hydrophobic interactions between itself and the biological samples<sup>70–75</sup>. To quantify these interaction forces, usually ranging from piconewtons to nanonewtons, AFM is operated in force-spectroscopy mode, in which the AFM stylus is made to approach the sample surface vertically, make contact with it and then retract from it. During approach and retraction, the vertical displacement of the AFM stylus and sample and the deflection (e.g., force) of the AFM cantilever are recorded in so-called force-displacement (FZ) curves. Subtraction of the cantilever deflection from the vertical displacement converts an FZ curve into a FD curve that is used to quantify the distance dependence of the interaction forces between the AFM stylus and the sample<sup>76</sup>.

In addition to quantifying the inter- and intramolecular interaction forces of biological systems, the AFM stylus can be used to probe mechanical properties. Therefore, the AFM stylus is indented into and retracted from the sample while the mechanical response of the sample is being measured<sup>76</sup>. Such indentation-retraction experiments can provide insight into the deformation, elastic modulus, viscoelasticity, pressure, material fatigue, adhesion, electrostatic properties and energy dissipation of a biological sample. Shortly after the discovery that interactions can be

detected between the AFM stylus and a sample, procedures were developed to use AFM-based force spectroscopy to characterize the specific binding of a ligand to its receptor. In this approach, the AFM stylus is functionalized with a receptor (or ligand) and a supporting surface with a corresponding ligand (or receptor)<sup>77–79</sup>. When the functionalized AFM stylus is brought into contact with the functionalized support, the receptor and ligand pair can bind. Retraction of the stylus from the support forces the specific bond formed between the receptor and the ligand to break. The force required to break the receptor-ligand bond is detected by the deflecting AFM cantilever.

### FD-based AFM combines AFM imaging and force spectroscopy

AFM operated in the imaging mode and in the force-spectroscopy mode opened the door to the nanoworld<sup>14</sup>, and the idea was quickly born to combine both in the so-called FD-based AFM. Invented about 20 years ago, FD-based AFM imaging has since been optimized to the point that it can image the architecture of complex biological systems, such as living cells, cellular membranes, model membranes, protein complexes, and viruses and nucleic acids; at the same time, it can quantify and map their various properties to piconewton and nanometer resolution<sup>11,80–86</sup>.

While raster-scanning the native biological sample, FD-based AFM records an array of FD curves (Fig. 1). For each pixel of the resulting AFM topography, the AFM records FD curves of the AFM stylus interacting with the sample at Ångstrom precision and piconewton sensitivity. These interaction forces are mapped, pixel by pixel, to the biological sample surface. From the resulting interaction map, a volume of forces is directly correlated to the sample topography<sup>11</sup>. Because a functionalized AFM stylus resembles a multifunctional nanoscopic toolbox, molecular interaction forces can be specifically detected and quantified<sup>15</sup>. This functionalization enables FD-based AFM to image complex biological systems and simultaneously quantify and map biological, chemical and physical properties to the molecular scale<sup>12</sup>.

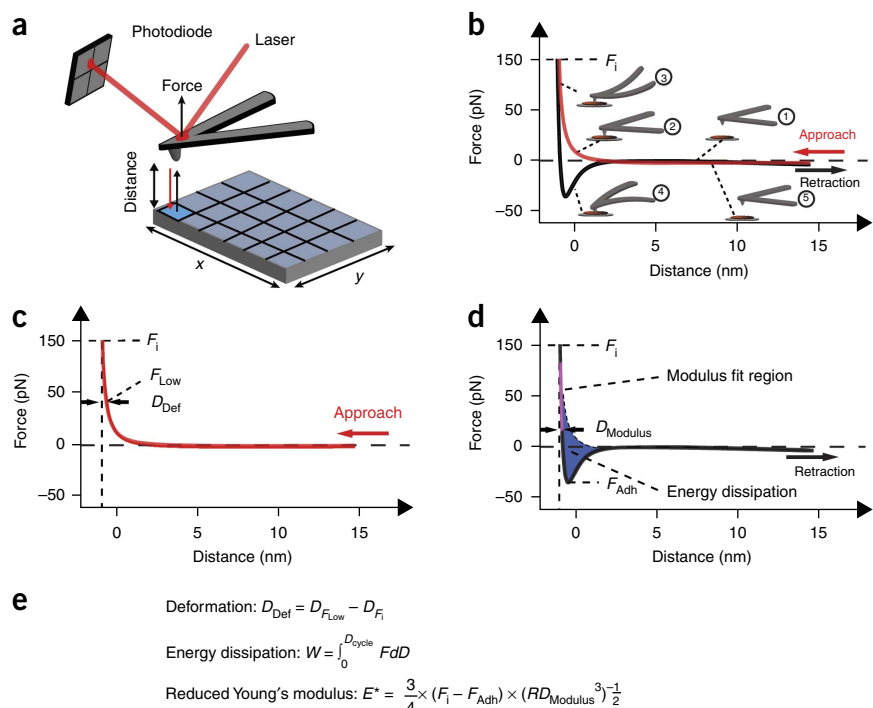
### FD-based AFM of native proteins approaching sub-nanometer resolution

For almost two decades, it has not been possible to obtain high-resolution (<5 nm) topographs of native proteins by FD-based AFM. Recent improvements in instrumental precision and data acquisition have enabled users to increase the lateral and vertical resolutions of FD-based AFM topographs to ~1 and ~0.1 nm on native proteins and protein complexes. Specimens analyzed at high resolution include the light-driven proton pump bacteriorhodopsin from *H. salinarum*<sup>87</sup>, the ferric hydroxamate uptake receptor (FhuA)<sup>88</sup> and OmpF porin<sup>89</sup> from *E. coli*, and pathological neurofibrils such as the  $\alpha$ -synuclein amyloid fibrils<sup>90</sup>, human islet amyloid polypeptide fibrils<sup>91</sup> and human tau fibrils<sup>92</sup> (Fig. 2). Illustrating the great sensitivity of the method, FD-based AFM of bacteriorhodopsin demonstrated that the native membrane protein surface can be contoured with sufficient spatial resolution to image single polypeptide loops in the fully extended state at low imaging forces (<75 pN) or in the reversibly compressed state at slightly elevated imaging forces (>75 pN)<sup>87,93</sup>.

### Protocol purpose and description

The purpose of this protocol is to simultaneously contour the surface and quantify the biophysical and biochemical properties of native proteins at high resolution (~1 nm) by FD-based AFM.

**Figure 1** | Principles of FD curve-based AFM for imaging and mapping multiple properties of biological samples. (a) In FD-based AFM, an AFM stylus is made to approach to and retract from a biological sample in a pixel-by-pixel manner to record FD curves. The high precision of the AFM enables the user to detect pixel sizes  $<1\text{ nm}^2$ , with a positional accuracy of  $\sim 0.2\text{ nm}$  and forces at piconewton ( $10^{-12}\text{ N}$ ) sensitivity. The height of every pixel of the final sample topography is determined by the stylus-sample distance, measured at a preset imaging force  $F_i$ . (b) Approach (red) and retraction (black) FD curves. Zero distance indicates the contact point of the tip and the sample. Analyzing the FD curves provides information such as the sample height, deformation, elasticity (Young's or DMT modulus), energy dissipation and adhesion. Cartoons depict the cantilever approaching to and retracting from the sample as follows: (1) noncontact, (2) initial contact and (3) repulsive contact regimes of cantilever stylus and sample detected in the approach FD curve. (4) Adhesion and (5) noncontact regimes recorded upon retracting the stylus and sample. (c) Information on the height and deformation of the biological sample can be extracted from the approach FD curve. The sample deformation  $D_{\text{Def}}$  is determined in this example as the stylus-sample distance  $D_{F_i}$  reached at the imaging force  $F_i$  (here 150 pN) minus the distance  $D_{F_{\text{Low}}}$  reached at a much lower force  $F_{\text{Low}}$  (here 45 pN). (d) Elastic modulus, adhesion force and energy dissipation can be extracted from the retraction FD curve. The adhesion force  $F_{\text{Adh}}$  is the minimum of the retraction FD curve. Energy dissipation  $W$  represents the blue shaded area between the approach and retraction FD curve. Stiffness  $k$  of the sample can be determined by the pink-colored slope ( $F = F_i - F_{\text{Mod}}$ )/ $D_{\text{Modulus}}$ . (e) Formulas suitable for extracting parameters described in c and d from FD curves. The sample elasticity  $E^*$  is estimated by using the DMT model<sup>143–145</sup>, with the imaging force  $F_i$ , the adhesion force  $F_{\text{Adh}}$ , the stylus-sample contact area  $R$  and the stiffness  $k = (F = F_i - F_{\text{Mod}})/D_{\text{Modulus}}$  of the biological sample.



We describe a protocol that can be applied to image membrane and water-soluble proteins. We have chosen to detail the protocol as applied to two prominent proteins, and we advise readers to implement this protocol in the study of either or both of these proteins to familiarize themselves with the procedure before analyzing their biological sample of choice. Bacteriorhodopsin from the purple membrane of *H. salinarum* is among the functionally and structurally best-studied membrane proteins that has also been intensively characterized by AFM imaging and force spectroscopy<sup>21,23,31,32,87,93–103</sup>. Because the purple membrane is commercially available and is a frequently used standard by many AFM groups, it is well suited to be used in a protocol. Many researchers use AFM to investigate fibrils assembled from water-soluble proteins such as actin, collagen, insulin, as well as intermediate

filaments, microtubules and neurofibrils. Currently, amyloid-like fibrillar aggregates involved in neurodegenerative diseases are intensively studied by AFM because their highly variable polymorphic structural and biophysical properties are particularly well resolved by the exceptional signal-to-noise ratio typical of AFM<sup>57,90,91,104,105</sup>. As a representative of such aggregates, we have chosen to describe the investigation of fibrils formed from the human tau protein, which is the main constituent of neurofibrillary tangles involved in Alzheimer's disease<sup>106,107</sup>.

In the following 'Experimental design' section, we describe bottlenecks and caveats that must be considered when imaging native single proteins and protein complexes by FD-based AFM at high resolution. We include description of the steps of sample preparation, AFM cantilever selection, and analysis

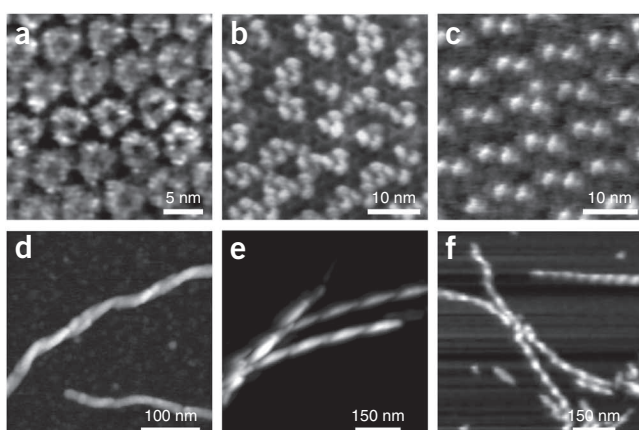


**Figure 2** | High-resolution FD-based AFM images of membrane proteins and fibrillated water-soluble proteins. (a) Cytoplasmic surface of purple membrane showing individual bacteriorhodopsin trimers<sup>87</sup>. (b) Densely packed assembly of OmpF porin trimers reconstituted into the lipid bilayer. Adjacent OmpF trimers either expose their extracellular or periplasmic surfaces. Highly protruding OmpF trimers (brighter) expose the extracellular surface, whereas the low-protruding OmpF trimers (darker) expose their periplasmic pores<sup>89</sup>. (c) Ferric hydroxamate uptake receptor (FhuA) from *E. coli* reconstituted into the lipid bilayer<sup>88</sup>. The high protrusions (brighter) represent single FhuA exposing their extracellular side, whereas lower donut-shaped features (darker) are FhuA exposing their periplasmic pores. (d) Amyloid-like fibrils assembled from full-length human tau<sup>92</sup>. (e) Fibrillating core fragment (hIAPP<sub>20–29</sub>) of the human islet amyloid polypeptide<sup>91</sup>. (f)  $\alpha$ -synuclein fibrils (E46K mutant form). Images adapted with permission from refs. 87,88,90–92, with copyrights from the American Chemical Society (refs. 89,90), from Elsevier (ref. 88), from Wiley and Sons (ref. 87) and from the National Academy of Sciences (USA) refs. 91,92.

## PROTOCOL

and interpretation of the FD-based AFM data. Our examples highlight that FD-based AFM can reveal surface structures at sub-nanometer resolution and structurally map at the same resolution biophysical properties, such as deformation, adhesion, energy dissipation and elasticity.

### Experimental design

**Critical sample immobilization.** For their investigation by FD-based AFM, water-soluble proteins can be simply adsorbed onto a supporting surface. A prerequisite to observe proteins in their native state is that the support does not modify their structure and/or impair their function. Hydrophilic supports are often better suited to maintain the native structure-function relationship of proteins than hydrophobic supports that can easily induce denaturation<sup>108,109</sup>. Native membrane proteins should reside in their native environment, the lipid membrane, which stabilizes the membrane protein and makes it much less sensitive to interfering interactions with the AFM support.

Membranes extracted from bacterial or animal cells or reconstituted protein membranes are 5–10 nm thick and extend laterally from ~0.2 to ~10 µm. For high-resolution FD-based AFM imaging, these membranes must be flatly adsorbed onto a support<sup>109,110</sup>. Membranes that do not spread properly or small proteoliposomes may be spread with the AFM stylus<sup>111</sup>. Muscovite mica and highly ordered pyrolytic graphite (HOPG) are widely used supports for AFM because they are atomically flat and clean after stripping off the top layers. Mica is negatively charged at neutral pH, shows a surface charge density ranging from −0.032 to −0.0025 C m<sup>−2</sup> that depends on the electrolyte concentration of the buffer solution<sup>112</sup>, and is hydrophilic and a good electrical insulator<sup>113</sup>. By contrast, HOPG exposes a hydrophobic surface and is a good conductor<sup>114,115</sup>. When combining AFM with light microscopy, glass slides have proven to be excellent supports. Depending on their sizes, the glass supports can be directly mounted onto the AFM or glued onto a larger carrier for mounting. As detailed in the PROCEDURE, we glue mica supports onto a thin Teflon foil, which is glued to the metal disc that is magnetically mounted to the piezoelectric scanner of the AFM. The hydrophobic Teflon spacer prevents the aqueous solution covering a hydrophilic sample support from spreading.

**Critical cantilever selection.** The choice of the cantilever depends on which forces, distances and kinetics of the biological system are to be investigated by FD-based AFM. For instance, measuring the interaction forces that are governed by single biomolecules, which typically range from 5 to 250 pN (refs. 116,117), requires soft AFM cantilevers (spring constant,  $k = \sim 0.01\text{--}0.5\text{ N m}^{-1}$ ). AFM cantilevers immersed in liquids are severely damped, thus lowering their quality (Q-) factor from 100 to 500 in air to <20. The Q-factor is a dimensionless parameter that is frequently used to describe the damping of the cantilever oscillations. The Q-factor can be calculated by dividing the resonance frequency of the cantilever through the width of the cantilever resonance curve. External acoustic, mechanical or electromagnetic frequencies (see also ‘Setting up the AFM’) within this width of the resonance curve can excite the cantilever. Thus, low Q-factors, such as those observed in buffer solution, imply that the cantilever can be excited at frequencies that are far removed from its resonance frequency. Consequently, if the movements

applied to the cantilever are too fast or close to the cantilever resonance frequency, the cantilever could be affected by hydrodynamic dragging or it could be excited, which requires complex algorithms to reconstruct the FD curves<sup>76,118,119</sup>. Therefore, as a rule of thumb, the resonance frequency of the cantilever in liquids should be at least five times higher than the frequency at which the cantilever is moved to record FD curves. Furthermore, to detect fast biomolecular interactions, cantilevers that show high resonance frequencies (>100 kHz) are needed<sup>120,121</sup>.

It is also important to note that the shape and size of the AFM stylus can limit the lateral resolution achieved by AFM. Generally, sharp AFM styluses with a small tip radius are recommended to achieve high resolution. Therefore, in the procedure described herein, we use styluses with a nominal tip radius of ~2 nm.

If FD-based AFM focuses on measuring the mechanical flexibility or stiffness of a sample, the spring constant (stiffness) of the cantilever should be similar to that of the sample<sup>84,122–124</sup>. If at the beginning of the experiment it is difficult to presume a value for the sample stiffness, a cantilever showing an intermediate stiffness (~0.1 N m<sup>−1</sup>) may be chosen. Subsequently, more suitable cantilevers should be used to refine the measurement. Ensure that the sensitivity of the AFM deflection detection system can impose limits in detecting small deflections (e.g., small forces ≤100 pN) that occur when applying stiff cantilevers ( $\gg 1\text{ N m}^{-1}$ ). When determining the stiffness of a biological sample, experimenters should consider that the sample’s mechanical properties are often structurally heterogeneously distributed. As biological systems ranging from lipids, proteins, membranes, and cells to tissues show quite heterogeneous structural features, the mechanical properties measured should be precisely assigned to structural details and to the direction alongside which the mechanical measurements are performed (e.g., perpendicular to the surface). Furthermore, because biological systems change structural properties dynamically, the functional state at which mechanical measurements were performed should be well defined.

The stiffness of biological systems can vary widely, with reported values ranging from <1 kPa to several hundreds of kPa for living animal cells<sup>125–127</sup>, from hundreds of MPa to several GPa for viruses<sup>85,128</sup>, from a few MPa to tens of MPa for protein membranes<sup>103,129,130</sup>, from MPa to GPa for single-membrane, water-soluble and fibrillar proteins<sup>87,92,123,129,131,132</sup> and from ~10 to ~500 MPa for lipid bilayers<sup>87,133,134</sup>. When determining the mechanical stiffness of a biological sample by FD-based AFM, you need to consider that this parameter can strongly depend on the velocity of the sensing AFM stylus (e.g., on the force-loading rate) and on electrolyte identity, electrolyte concentration and pH of the buffer solution<sup>103</sup>.

As the cantilever deflection sensitivity can change during the experiment, we recommend calibrating the deflection sensitivity of the cantilever before and after recording FD curves. The deflection sensitivity of the cantilever is best determined by pressing the cantilever stylus to a stiff support (e.g., mica or glass and not the biological system). Changes in the cantilever deflection sensitivity can have different origins. On the one hand, the position of the laser on the cantilever can drift (for instance, owing to temperature changes). On the other hand, the reflectivity of a cantilever can change over the course of an AFM experiment. Alternatively, changes in the reflectivity of the cantilever can occur owing to

cantilever contamination or to damages of the reflective coating layer of the cantilever. For regular AFM experiments, variations of the cantilever deflection sensitivity of  $\approx 5\text{--}8\%$  within several hours can be considered acceptable.

**Critical FD curve analysis.** To record an FD curve, the AFM brings the stylus and the sample into contact and separates them again (Fig. 1a). For the accurate analysis of FD curves, it is often necessary to define the stylus-sample distance and thus the contact point between the AFM stylus and the sample<sup>76</sup>. However, accurately defining this contact point becomes increasingly complex when you are working with native biological systems that are very soft and that have structurally heterogeneous and dynamic properties. Thus, in most cases, the contact point between the AFM stylus and the biological sample is only estimated in FD curves (Fig. 1b). Fortunately, the error associated with this approximation is negligible for many AFM applications.

As FD curves record interaction forces between the AFM stylus and the sample, the analysis of FD curves can provide insight into the nature of these interactions<sup>76</sup>. Accordingly, physical forces of interactions resulting from Coulomb forces, van der Waals forces, electric double-layer repulsion, Pauli repulsion, hydrophobic attraction, solvation forces and water layering have been characterized by using FD curves<sup>70–76</sup>. In addition, biochemical forces stabilizing covalent bonds, ligand-receptor pairs, biopolymers, nucleic acids, membrane and water-soluble proteins, cellular membranes and lipid bilayers have been quantified by recording FD curves<sup>77,78,97,135–138</sup>. Last but not least, FD curves also enable you to link the mechanical properties and functions of biological systems<sup>47,65,139,140</sup>.

Some of the sample properties such as deformation, stiffness, elastic modulus, adhesion and energy dissipation that can be extracted from FD curves are highlighted in Figure 1c,d. Upon indentation of the stiff AFM stylus into the soft biological sample, the deformation of the AFM stylus can be neglected. Accordingly, the deformation of the much-softer biological sample can be determined by subtracting the distances measured at two different forces indenting the AFM stylus into the sample (Fig. 1c). The mechanical stiffness (e.g., spring constant) of the sample can be extracted from a linear slope of the FD curve (from either the approach or retraction curve) that is recorded when the AFM stylus and the sample are in contact (Fig. 1d). On the basis of different elastic contact models (e.g., the Derjaguin-Muller-Toporov (DMT) model) used to estimate the contact area between the AFM stylus and the sample, the mechanical stiffness can be used to determine the elastic Young's modulus<sup>141–145</sup>. Whereas the adhesion force

between the AFM stylus and the sample is the minimal force of the retraction FD curve, the energy of the sample dissipating upon separating the AFM stylus is related to the difference area between the approach and retraction FD curve (Fig. 1d).

### Applicability and limitations of the protocol

This protocol is demonstrated for the characterization of membrane protein bacteriorhodopsin and of amyloid-like fibrils assembled from water-soluble human tau, but it is amenable to the study of most membrane and water-soluble proteins regardless of their origin. Because our protocol is limited to the characterization of single native proteins *in vitro*, the forthcoming great challenge will be to characterize single proteins in their native environment of the living cell or tissue. Only then will we be able to reach the goal of determining how proteins work in the cellular context and how cells control proteins to function as required. In this regard, we see our protocol as an important step toward structurally quantifying the unique properties of native proteins. Importantly, methods that enable the characterization of the physical (including mechanical), chemical and biological properties of proteins and protein complexes at nanoscale resolution are becoming increasingly important as part of the investigative toolkit in life sciences and nanotechnology. This is because quantitative high-resolution microscopy methods can access properties that are invisible to conventional light microscopy and structural biology approaches, and they can be combined with chemical (e.g., chemical perturbation, drugs) and genetic (e.g., genetic perturbation, mutation) approaches to characterize structural and functional phenotypes.

In our protocol, we describe how to achieve high-resolution FD-based AFM topographs approaching a lateral resolution of  $\sim 1\text{ nm}$  and a vertical resolution of  $\sim 0.1\text{ nm}$ . The simultaneously recorded mechanical properties of the native protein show the same resolution. Recent procedures developed to chemically and biologically functionalize the AFM stylus<sup>15,84,86,122</sup> enable you to obtain FD-based AFM topographs of biological specimens and to simultaneously map specific chemical and biological interactions (e.g., ligand binding, chemical groups, substrate transport). These procedures must be further adapted to be applicable for high-resolution ( $\sim 1\text{ nm}$ ) FD-based AFM imaging of proteins. However, as described in our protocol, FD-based AFM is readily applied to obtain high-resolution topographs and multiparametric maps of native proteins. Thus, we believe that FD-based AFM, as described here, will lead to further discoveries at the interface of molecular biology, physiology and biophysics.

## MATERIALS

### REAGENTS

- Analytical-grade buffers (sodium phosphate dibasic,  $\text{Na}_2\text{HPO}_4$ ; Sigma, CAS no. 7558-79-4; potassium phosphate monobasic,  $\text{KH}_2\text{PO}_4$ ; Sigma, CAS no. 7778-77-0; tris(hydroxymethyl)aminomethane, Tris; Sigma, CAS no. 77-86-1)
- Analytical-grade electrolytes (NaCl; Sigma, CAS no. 7647-14-5; KCl, Merck, CAS no. 7447-40-7)
- DL-DTT (DTT; Sigma, CAS no. 3483-12-3)
- Hydrochloric acid, 37% (wt/wt) (HCl; Sigma, CAS no. 7647-01-0)
- Sodium azide ( $\text{NaN}_3$ ; Sigma, CAS no. 26628-22-8) **! CAUTION**  $\text{NaN}_3$  is highly toxic and should be handled accordingly.
- Glycerol (Sigma, CAS no. 56-81-5)
- Commercially available dishwashing detergent

- Ultrapure isopropanol, 99.5% (vol/vol) (Fluka, CAS no. 67-63-0)
- Ultrapure ethanol, 99.7% (vol/vol) (Fluka, CAS no. 64-17-5)
- Purple membranes extracted from *H. salinarum*<sup>146</sup> (Munich Innovative Biomaterials) or membranes of choice (see Reagent Setup)
- Fibrils assembled from full-length or truncated human tau<sup>147</sup> (see Reagent Setup, or use amyloid fibrils of your choice)
- PBS (see Reagent Setup)
- Adsorption buffer for purple membrane (see Reagent Setup)
- Imaging buffer for purple membrane (see Reagent Setup)
- Adsorption buffer for human tau fibrils (see Reagent Setup)
- Imaging buffer for human tau fibrils (see Reagent Setup)
- Nanopure water ( $\sim 18\text{ }\Omega\text{ cm}^{-1}$ , e.g., Purelab Ultra) **▲ CRITICAL** Working with nanopure, double-distilled or ultrapure water is crucial to avoid

## PROTOCOL

residual electrolytes and contamination of the sample by molecular debris found in normal and deionized water.

### EQUIPMENT

- Mica punch set (e.g., 'Punch and die', Precision Brand Products, UPC no. 40105)
- Steel disc (e.g., AFM metal specimen disc, 12 mm, Ted Pella, prod. no. 16208) or other suitable AFM sample holder (e.g., glass sample holder)
- Teflon foil of thickness below 0.2 mm
- Stereo light microscope for cantilever mounting (Stemi DV4, Zeiss)
- Non-magnetic tweezers (e.g., Dumont no. 7 forceps, 0.17 mm × 0.1 mm, 11.5 c, art. no. 11297-0)
- Muscovite mica (Mica New York Corporation) cleaved to thickness less than 0.5 mm
- Scotch tape
- Teflon-compatible glue (e.g., Loctite 770/406) and chemically inert two-component epoxy glue (e.g., Araldite Rapid)
- Air-gun with filter and tubing to connect to the nitrogen outlet (Air Gun GF-30A and tube connector, Skan)
- Active or passive vibration isolation, acoustic noise isolation (e.g., noise-absorbing hood or glass bell)
- Mechanical vibration analyzer (vibration analyzer VA-2, Table Stable)

▲ **Critical** Vibrational and acoustic isolation is crucial in these experiments.

- FD-based AFM with fluid cell (e.g., Nanowizard 3 operated in the QI mode (JPK Instruments), Multimode 8 operated in the PeakForce QNM mode (Bruker or from other manufacturers)) ▲ **Critical** AFM choice is crucial in these experiments. AFM systems from different manufacturers come with different specifications, such that they may or may not allow, for example, adjusting the frequency and velocity at which the piezo of the AFM moves the cantilever to record FD curves, the number of pixels scanned per image (at least 256 × 256), the number of data points recorded per FD curve (at least 256 points), the contact time of AFM stylus and sample and the resolution in z- and xy-scanning directions. Please note that commercial AFMs (e.g., Asylum, Bruker, JPK) come with their own software tools that show major differences in the ability to extract and process FD curves. However, the FD curve maps can be exported and post-processed by using third-party software such as MATLAB or Origin.
- ▲ **Critical** Make sure that the AFM keeps the maximal force applied to the sample accurate within a few piconewtons. The maximal scan size should be >30 µm to allow searching good sample areas that are suitable for high-resolution imaging (i.e., protein membranes or protein assemblies).
- High-resonance rectangular-shaped Si<sub>3</sub>N<sub>4</sub> cantilever (Olympus, 0.1 N m<sup>-1</sup>, 28 kHz in water) or V-shaped Si<sub>3</sub>N<sub>4</sub> cantilever with a sharpened silicon stylus having a nominal tip radius approaching 2 nm (Bruker, 0.7 N m<sup>-1</sup>, 30 kHz in water) ▲ **Critical** Cantilever choice is a crucial parameter in these experiments. For long-timescale mechanics experiments, we recommend silicon or silicon nitride cantilevers. Metal-coated cantilevers quite frequently suffer from extensive drift due to the difference in thermal expansion coefficient between the silicon (or silicon nitride) and metal layers.
- Sterile wipes (Kimtech, Kimberly Clark, prod. no. 05511)
- Weighing paper (Macherey-Nagel, cat. no. 186002)

### REAGENT SETUP

**Purple membrane of *H. salinarum*** Prepare 100-µl aliquots of purple membranes (0.25 mg ml<sup>-1</sup>) in nanopure water containing 0.01% (vol/vol)

NaN<sub>3</sub>. Freeze them and store them at -80 °C until needed. At -80 °C, the samples are stable for >12 months. Before starting the experiment, transfer one such aliquot to a 4 °C freezer, until its temperature is equilibrated. At 4 °C, the samples are stable for several weeks.

**Human tau fibrils** Assemble tau fibrils from recombinant human protein as described in ref. 147 and store them in PBS containing 1 mM DTT and 0.01% (vol/vol) NaN<sub>3</sub> at 4 °C. ▲ **Critical** Tau fibrils are stable for weeks when they are kept at 4 °C. For longer storage times, up to several months, store the fibrils at -20 °C or -80 °C. ▲ **Critical** Please note that we recommend that researchers apply the present procedure to either bacteriorhodopsin from *H. salinarum* or tau fibrils, as a way to familiarize themselves with this protocol (see INTRODUCTION), not necessarily to both proteins.

**AFM adsorption and imaging buffer solution** Prepare all buffers with nanopure water, analytical-grade buffer and electrolytes. Preferably use freshly prepared buffers and do not store buffers for more than 1 week. Rinse freshly cleaned bottles and measuring cylinders several times with nanopure water to remove debris. Make sure that all items that come in contact with the electrolyte (e.g., spatula and weighting paper) are very clean so that they cannot add contaminants. To adsorb the biological sample to a supporting surface, in most cases the electrostatic double-layer repulsion between the sample and support must be overcome<sup>110,148</sup>. This can be facilitated by increasing the electrolyte concentration, electrolyte valence or by adjusting the pH of the buffer solution. Once the sample has been adsorbed to the support, the buffer solution may be changed to a more physiological one. High-electrolyte buffers (>150 mM monovalent electrolyte) are preferred to adsorb protein membranes and complexes to the negatively charged mica surface. Divalent ions (i.e., MgCl<sub>2</sub>) can be added to more efficiently compensate the electrostatic repulsion between mica and the biological sample. ▲ **Critical** The biological samples, supports and AFM stylus are easily contaminated by particles and macromolecules. Thus, the AFM adsorption and imaging buffer solution should be clean of contaminants. Every surface (e.g., fluid cell, pipette tips, buffer flask) that is in contact with the buffer solution is a potential source of contamination and should be cleaned. Therefore, clean these surfaces thoroughly and use only nanopure water and analytical-grade chemicals. A good control to check whether the buffer solution is sufficiently clean is to image freshly cleaved mica in the buffer solution by FD-based AFM at very low imaging forces and a scan size of 100–500 nm. Only if the mica shows no molecular debris may you conclude that the buffer solution and the surfaces that are in contact with the buffer solution are indeed clean.

**PBS** Combine 137 mM NaCl, 2.7 mM KCl, 10 mM Na<sub>2</sub>HPO<sub>4</sub> and 1.8 mM KH<sub>2</sub>PO<sub>4</sub> (pH 7.4). This can be stored for 1 week at room temperature (20–25 °C).

**Adsorption buffer for purple membrane** Combine 300 mM KCl and 10 mM Tris-HCl (pH 7.8). This can be stored for 1 week at room temperature.

**Imaging buffer for purple membrane** Mix 150 mM KCl and 10 mM Tris-HCl (pH 7.8). This can be stored for 1 week at room temperature.

**Adsorption buffer for human tau fibrils** Mix 150 mM KCl and 10 mM Tris-HCl (pH 7.8). This can be stored for 1 week at room temperature.

**Imaging buffer for human tau fibrils** Combine 50 mM KCl and 10 mM Tris-HCl (pH 7.8). This can be stored for 1 week at room temperature.

## PROCEDURE

### Preparation and mounting of supports ● TIMING 2–8 h

- 1| Punch Teflon foil into a disc shape with a diameter of 1.5–2 cm. Clean the resulting Teflon disc with isopropanol and dry it with sterile tissue paper.
- 2| Glue the Teflon disc to a steel disc (or, depending on the AFM used, to another suitable support, such as a glass sample holder) with Teflon glue (Loctite 770/406).
- 3| Punch thin (<0.5 mm) mica sheets into discs with a diameter of 0.5–1 cm. Irregular reflections from mica discs indicate whether the layered material has been distorted by punching. Glue undistorted mica onto the Teflon disc by using epoxy glue (Araldite Rapid).

▲ **CRITICAL STEP** Epoxy glue should be uniformly distributed between mica and Teflon and completely hardened. The glue should be devoid of air bubbles, which can cause vibration or drift on the nanometer scale.

4| Clean all contact surfaces with isopropanol and/or ethanol. Be aware that small particles or liquid between the support and AFM can cause vibrations and drift.

#### Setting up the AFM ● TIMING 1–8 h

5| Place the AFM into a temperature-stabilized room or hood. If neither is available, try to keep the temperature variation of the AFM room at minimum.

6| Isolate the AFM from mechanical and acoustic noise.

▲ **CRITICAL STEP** For the high-resolution imaging of native proteins, the AFM should be placed on an actively or passively vibration-damped table. To achieve acoustic isolation, the best option is to place the AFM in a glass bell or an acoustic hood. Avoid the cables connecting controller and AFM to couple mechanical or acoustic noise.

▲ **CRITICAL STEP** Mechanical and acoustic noise can impair high-resolution FD-based AFM imaging of native proteins and the detection of very low forces approaching the piconewton scale. Such noise may be traced by using vibrational or acoustic noise analyzers or by recording the deflection of the free AFM cantilever and of the cantilever in contact with the mica support.

7| Isolate the AFM from sources that may cause electronic noise. To avoid ground loops, which can be a major source of electrical noise, make sure that all instruments that are part of the AFM are connected to the same electrical ground.

▲ **CRITICAL STEP** Electrical noise impairs high-resolution AFM imaging and the detection of very low forces approaching the piconewton scale. To remove electrical noise, look for possible sources of electronic noises by switching off the devices individually and checking their effect on the perceived noise. Electrical noise may be detected by sensing the electrical input and output signals of the AFM or by deflecting the laser beam from a solid support.

8| Turn on the AFM and associated instruments. The laser detecting the position of the cantilever and the control of the electronics of the AFM usually require an equilibration time to operate in a stable manner. To avoid 'drift' before equilibration is achieved, the AFM and associated instruments may be turned on for several hours before performing the measurements.

#### Choosing the AFM cantilever and cleaning the AFM components ● TIMING ~1 h

9| Choose a suitable cantilever, keeping in mind that this choice determines whether proteins can be imaged at high resolution in the unperturbed state and whether the mechanical properties of the sample can be detected and qualified correctly (see 'Critical cantilever selection'). Briefly, the cantilever spring constant, resonance frequency (in liquid) and tip radius of the stylus must be selected properly for each experiment. Generally, a tip radius  $\leq 10$  nm is recommended for FD-based AFM imaging approaching a resolution in the nanometer range. If the sample stiffness is unknown at the beginning of the experiment, a cantilever with an intermediate stiffness ( $\sim 0.1$ – $0.5$  N m $^{-1}$ ) may be chosen. Subsequently, more suitable cantilevers should be used to refine the measurement. To image bacteriorhodopsin and human tau fibrils, we advise using Bruker cantilevers with styluses having a nominal tip radius of  $\sim 2$  nm and a spring constant of 0.7 N m $^{-1}$  (see Equipment). It has been proven that these cantilevers can yield high-resolution AFM topographs of both biological samples. However, softer cantilevers from Olympus (0.1 N m $^{-1}$ , see Equipment) can yield a higher signal/noise ratio of the FD curves and may more accurately determine the mechanical parameters of a soft biological sample.

▲ **CRITICAL STEP** The acquisition frequency of the FD curves must be chosen by taking into account the cantilever properties (see 'Critical cantilever selection'). Ideally, recording topographs of a test sample (such as purple membrane) helps identify cantilevers that are suitable for sub-nanometer imaging.

10| Clean all components that will be in contact with the buffer solution during AFM imaging, such as the AFM fluid cell and sample support. If possible, clean these components using commercially available dishwashing detergent and filtered nanopure water. Rinse the components with ultrapure ethanol and nanopure water at least three times, and then dry the components using clean (e.g., filtered) nitrogen gas.

▲ **CRITICAL STEP** Do not dry the AFM components with pressurized air, as it is in most cases not sufficiently clean and contains oil, particles and so on from the compressing process. These particles can contaminate the buffer solution and the sample.

#### Adsorption of membranes or tau fibrils ● TIMING ~1 h

11| Place the sample support onto the support holder of the AFM.

▲ **CRITICAL STEP** Avoid tilting the support in the process.

## PROTOCOL

12| Cleave the mica disc uniformly by using Scotch tape. To achieve this goal, place a section of Scotch tape on the mica disc so as to cover its entire surface, and then peel it off carefully.

13| While peeling off the tape from the mica disc, make sure that the entire disc cleaves. Do so by looking at the peeled off mica glued to the tape. If cleavage has not been done properly, some glue from the tape may remain on the mica.

▲ **CRITICAL STEP** As it will come in contact with the buffer solution, any glue left on the mica surface will contaminate your sample.

14| Watch the mica during cleavage with the tape and make sure that no loosely attached mica sheets flip back to the mica disc. Such weakly attached mica sheets severely impair AFM imaging.

15| Prepare the biological sample solution according to option A, if the protein to be investigated is bacteriorhodopsin, or option B, if the biological sample is composed of tau fibrils. Please note that in order to adsorb a different protein (or nucleic acid) sample it may be necessary to adjust the pH, electrolyte type and electrolyte concentration of the adsorption buffer to overcome the electrostatic double-layer repulsion between the sample and the support. A detailed overview on how to adsorb biological macromolecules to different supports is given in ref. 110.

**(A) Preparation of the biological sample for bacteriorhodopsin characterization**

(i) Dilute the purple membrane stock solution in adsorption buffer to  $\sim 10 \mu\text{g ml}^{-1}$  and place  $\sim 30 \mu\text{l}$  of it onto the freshly cleaved mica for 15–30 min (refs. 21,110).

**(B) Preparation of the biological sample for the characterization of tau fibrils**

(i) Dilute the fibril solution in adsorption buffer to a final concentration of  $\sim 3 \mu\text{g ml}^{-1}$  and place  $\sim 10\text{--}20 \mu\text{l}$  of it onto the freshly cleaved mica for 10–20 min (refs. 57,92).

**? TROUBLESHOOTING**

16| Remove the adsorption buffer on the mica with a pipette. Rinse the sample adsorbed on the mica surface with imaging buffer several times ( $>5$ ) to remove excess and weakly attached membranes and proteins. Finally, add  $30 \mu\text{l}$  of imaging buffer on the mica.

17| Place the AFM cantilever in the AFM fluid cell.

▲ **CRITICAL STEP** Make sure that the cantilever is attached tightly to the fluid cell and that the spring holder is not loose. Check this by gently trying to move the fixed cantilever with sharp tweezers. Any loose motion of the cantilever will transfer into drift and the appearance of hysteresis during scanning.

18| Mount the sample and the AFM fluid cell so that the AFM cantilever is immersed in buffer solution. After this, thermally equilibrate the AFM. During equilibration, which may take 10–60 min, you may focus the laser beam onto the cantilever end and adjust the photodiode signal. A stable diode signal indicates minimum thermal drift.

▲ **CRITICAL STEP** To avoid large thermal gradients within the AFM, make sure that the buffer solution is at the same temperature as the AFM. Monitoring the deflection signal of a free cantilever is a simple way to check for thermal drift. When this drift does occur, the deflection signal easily changes within 1 min, and it is advisable to wait until the deflection signal approaches a stable value. When working in liquids with soft cantilevers ( $\sim 0.05 \text{ N m}^{-1}$ ), the thermal drift of the cantilever can be pronounced at the beginning of the experiment. If the AFM is not thermally equilibrated, stable imaging at low applied forces ( $<100 \text{ pN}$ ) will be impaired (see Step 25).

**? TROUBLESHOOTING**

19| (Optional) If the AFM does not thermally equilibrate within the time frame indicated in Step 18, look for the reason for this occurrence. For this purpose, watch whether a cantilever mounted onto the AFM drifts either in air or in water. If it drifts in both phases, the drift is instrumental or thermal. Next, remove any possible heat source from around the AFM. If the drift is not eliminated at this point, contact the AFM manufacturer, as the drift may be instrumental. If the cantilever drifts when immersed in water, but it does not do so in air, the cantilever may be defective or contaminated.

**Calibration and checking for contamination of the cantilever** ● **TIMING 10 min**

20| To calibrate the cantilever, first position it over a stiff sample, such as the support (mica), on which no (softer) biological samples have been adsorbed. Then conduct the approach and retraction cycles of the AFM cantilever by pushing the AFM stylus to the support, and record the FD curves. As the vertical displacement of the piezoelectric scanner is known during these cycles, it is possible to determine how much the cantilever has to deflect to generate a certain voltage difference of the photodiode. Because the support (mica, in this case) stiffness is orders of magnitude higher than that of

the cantilever, the deformation of the support is negligible compared with the deflection of the cantilever. This relation between the cantilever deflection and the voltage difference of the photodiode is described as cantilever deflection sensitivity. Usually, commercially available AFMs come with software routines that enable the calculation of the deflection sensitivity from FD curves.

▲ **CRITICAL STEP** Usually, the factor used to convert the volts measured by the AFM photodiode to nanometers of the cantilever deflection is referred to as deflection sensitivity. The deflection sensitivity depends on many parameters, including the type of cantilever and how it is mounted. Thus, the deflection sensitivity must be determined each time a cantilever is mounted or remounted and every time after the laser beam has been refocused. It is crucial to conduct these measurements as precisely as possible, because they will determine how accurately forces can be measured by AFM.

▲ **CRITICAL STEP** When recording FD curves, apply as little force as needed (<150 pN) to reach a linear regime in the cantilever deflection versus vertical displacement of the piezoelectric scanner and to avoid damaging the AFM stylus.

### ? TROUBLESHOOTING

**21** To complete the calibration process, determine the cantilever's spring constant ( $k$ ). For this purpose, use the relevant AFM software, which enables users to infer  $k$  through the analysis of thermal noise. Please note that, in order to avoid surface-induced artifacts, the cantilever must be withdrawn to a distance of at least 100  $\mu\text{m}$  from the support.

▲ **CRITICAL STEP** Calibration of the cantilever is necessary to convert the photodiode voltage detecting the cantilever deflection into force. The photodiode voltage (V) is multiplied by the cantilever deflection sensitivity ( $\text{nm V}^{-1}$ ) to yield the cantilever deflection (nm), which is multiplied by the cantilever spring constant  $k$  ( $\text{N m}^{-1}$ ) to calculate the force deflecting the cantilever (N). Most manufacturers provide nominal  $k$  values for their cantilevers. The  $k$  value can be estimated from the dimensions of the cantilever and the mechanical properties of the constituent material<sup>149</sup>. However, calibrated  $k$  values of cantilevers frequently differ from the nominal values by a factor up to 3. Most AFM software packages enable the determination of the  $k$  value of a cantilever by using the thermal noise method, which records the cantilever's thermal fluctuations and uses the data thus obtained in conjunction with the equipartition theorem<sup>150–152</sup>. Essentially, the theorem relates the absolute temperature of a system with its average energy. The thermal noise method is the most versatile and implementable method of cantilever calibration in liquids<sup>153</sup>. A high estimate of the error in determining the cantilever spring constant is 20% (ref. 153). It may be argued that other calibration methods are more accurate, but the extra effort required to apply such methods makes them rather unfeasible.

**22** Record an FD curve directly after engaging the stylus, as this may show whether the stylus or the supporting surface is contaminated. FD curves with sharp transitions (Fig. 3a,b) indicate clean preparations. By contrast, FD curves recorded with a contaminated sample and/or AFM stylus frequently show irregular and irreproducible FD patterns (Fig. 3c). A good way to check whether the AFM stylus has been contaminated is to record FD curves on a clean freshly cleaved mica surface (nothing should coat the mica). If the FD curve looks as it does in Figure 3a,b (ref. 76), the AFM stylus is probably not contaminated.

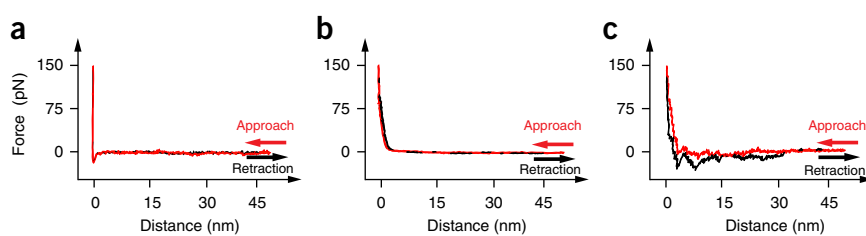
▲ **CRITICAL STEP** Loosely bound molecules can contaminate the AFM stylus, and eventual contaminants influence the interaction of the AFM stylus with the biological sample. Therefore, the sample, buffer solution and fluid cell have to be clean; if they are not, the AFM stylus will be contaminated.

### ? TROUBLESHOOTING

#### Low-resolution FD-based AFM imaging ● TIMING ~1 h

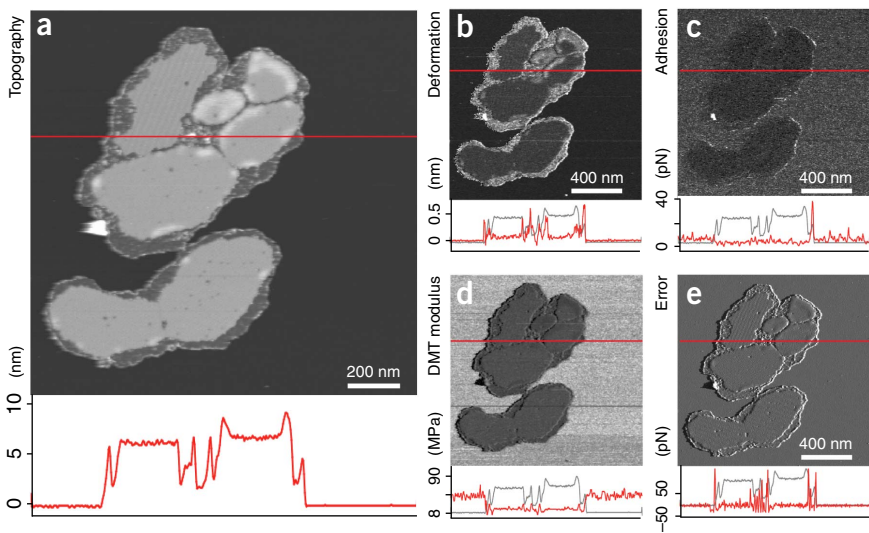
**23** Engage the AFM at the lowest possible force ( $\ll 100$  pN), with optimal (fast) feedback gain and in a small scanning area (<10 nm). If the AFM fails to engage, FD curves record no transitions and AFM images contain no information other than noise.

**Figure 3** | Approach and retraction FD curves recorded on supporting surfaces. (a) FD curves recorded in buffer solution on a clean and mechanically stiff support. The sharp transition close to the contact area (0 nm) indicates a clean AFM stylus (here,  $\text{Si}_3\text{N}_4$ ) approaching a clean support (here, mica), and it indicates that both materials are mechanically stiff. The good agreement between approach and retraction FD curves shows no hysteresis and thus also indicates that the AFM system has been set up properly and that the AFM stylus and sample are not contaminated. (b) FD curves recorded in buffer solution on a clean, mechanically flexible sample. The relatively smooth transition around the contact area and the missing hysteresis indicate that a clean AFM stylus (here,  $\text{Si}_3\text{N}_4$ ) approaches a clean support (here, purple membrane) and that, in this case, the support is mechanically softer than the stylus. (c) FD curves recorded in buffer solution using a contaminated AFM stylus. The discontinuous transition and the hysteresis between approach and retraction FD curves indicate a contaminated AFM stylus and/or mica surface. FD curves were recorded in buffer solution (150 mM KCl, 10 mM Tris-HCl, pH 7.6), by applying an imaging force of 150 pN, a cantilever oscillation amplitude of 50 nm and a frequency of 2 kHz, as well as 20.5 data points per nm.



## PROTOCOL

**Figure 4** | FD-based AFM images of purple membrane adsorbed onto mica. (a–e) AFM topography (a), deformation map (b), adhesion map (c), DMT modulus map (d) and force error map (e). (a–e) Vertical scales correspond to 10 nm (a), 0.5 nm (b), 40 pN (c), 8–90 MPa (d) and from –50 pN to 50 pN (e). The red lines in the AFM images (a–e) indicate where the vertical profile shown below each image has been extracted. Gray lines in panels b–e show the topographic profile recorded in a. The topography shows densely packed patches of bacteriorhodopsin surrounded by thin rims of a lipid bilayer. Data were recorded in buffer solution (150 mM KCl, 10 mM Tris-HCl, pH 7.8), by applying an imaging force of 140 pN, a cantilever amplitude of 40 nm, a frequency of 2 kHz and a scanning frequency of 1 Hz per line. Note that a soft cantilever was chosen to measure the Young's modulus of purple membrane, which gives a wrong estimate of the Young's (DMT) modulus of mica (see 'Critical cantilever selection').



To engage the AFM, increase the force slightly (through successive ~10 pN steps) as many times as needed to find the lowest possible force required to engage your AFM stylus.

**▲ CRITICAL STEP** Forcing the AFM stylus to approach the support may damage the AFM stylus. Such damage occurs by pressing the AFM stylus at very high force onto the support ( $\gg 500$  pN). In addition, the feedback loop that limits the maximum force of the AFM stylus contacting the support should be set as fast as possible. Optimal gains are reached just below the gains that turn the feedback loop unstable and cause the AFM deflection error and height signals to oscillate.

### ? TROUBLESHOOTING

**24** | Image the sample by using the FD-based AFM mode. Adjust the lowest possible imaging force as described in Step 23 and optimize feedback gains. Depending on the piezoelectric scanner, one can obtain overview images at sizes ranging from ~10 to 50  $\mu$ m (Fig. 4). Large overview images should be obtained at minimal forces ( $\ll 500$  pN) and scanning line frequencies (1–2 Hz), with a maximal feedback gain and at a resolution (i.e., pixel size) sufficient to observe structural details of the biological sample. The vertical amplitude of the FD curves should be rather high ( $\approx 40$ –60 nm) to compensate for larger obstacles and the tilt of the support. The scanning angle may be adjusted to compensate for the tilt of the support. Feedback gains are optimal if they are at their maximum possible values without causing the AFM cantilever (or piezoelectric scanner) to oscillate during imaging at minimal forces. Keep the scanning speed low to avoid crashing the AFM stylus into highly corrugated objects. If the sample is flat, the scanning speed may be increased.

**▲ CRITICAL STEP** Throughout imaging, the force applied to the AFM cantilever must be kept at the minimum possible values. Slightly increasing the forces deforms the flexible structural regions of the proteins reversibly, until the forces are so high that deformation becomes irreversible<sup>93,103,111</sup>. In many cases, the applied forces have to be adjusted to optimize the topographic contrast without deforming the sample.

### ? TROUBLESHOOTING

**25** | (Optional) To make sure that the imaging process is not destructive for the soft protein sample, we recommend repeatedly imaging the same area of the sample. When sample deformation occurs, the imaging force may be reduced, the vertical amplitude moving the cantilever up and down increased, the scanning line frequency decreased and/or the feedback gains optimized. Please also note that a large hysteresis between trace and retrace scanning lines can have several causes: first, the cantilever may not be attached properly to the fluid cell; second, the support may show defects (i.e., bubbles, soft glue, mica badly cleaved); and third, the feedback gains may be too low. If no membranes (or fibrils) are found on the support, excessive imaging forces may have been chosen, or the feedback of the AFM cantilever may have been incorrectly adjusted. Alternatively, the concentration of the purple membrane (or tau fibrils) in the adsorption buffer may be too low.

**26** | (Optional) If you observe purple membranes forming stacks or aggregates, ultrasonicate the adsorption buffer containing the purple membrane for 1–3 min and repeat adsorption. Ultrasonication dissolves purple membrane aggregates but not purple membrane. Be aware that you may not ultrasonicate other protein samples, as they are usually much less stable than purple membrane.

### ? TROUBLESHOOTING

#### High-resolution FD-based AFM imaging ● TIMING 2–4 h

**27** | After performing imaging overviews (Steps 23–26), zoom in on a selected area of your biological sample (Fig. 5). Preferably, this area should show flatly adsorbed purple membrane patches or tau fibrils. Adjust the amplitude by vertically

**Figure 5** | High-resolution FD-based AFM of the extracellular purple membrane surface reveals sub-structural details of bacteriorhodopsin trimers. **(a,b)** Raw data (**a**) and average (**b**) AFM topography of bacteriorhodopsin trimers. **(c,d)** Raw data (**c**) and average (**d**) DMT modulus map. **(e,f)** Raw data (**e**) and average (**f**) deformation map. Averages were calculated from unit cells extracted at the positions from which the bacteriorhodopsin trimers were observed in the topograph<sup>87</sup>. **(a–f)** Vertical scales of 0–1.0 nm (**a,b**), 5–18 MPa (**c,d**) and 0.2–1.2 nm (**e,f**). The red lines in the AFM images indicate where the vertical profile shown below each image has been extracted. Gray lines in **c–f** show the topographic profile recorded in **a** and **b**. Data were recorded in buffer solution (150 mM KCl, 10 mM Tris-HCl, pH 7.8), by applying an imaging force of 45 pN, a cantilever amplitude of 14 nm, a frequency of 2 kHz and a scanning frequency of 0.77 Hz per line.

moving the AFM stylus until the topographic contrast (or other contrast) is optimal. At the beginning, the amplitude may be adjusted roughly to the expected height of the object (e.g., membrane proteins, 4–15 nm; protein fibrils, 10–25 nm). Please note that at too-high amplitudes the force feedback may be impaired and the biological sample may be damaged.

#### ? TROUBLESHOOTING

**28** | For high-resolution FD-AFM imaging, the imaging force needs to be minimized to detect the smallest possible structural details with a minimal deformation of the soft biological sample. Therefore, reduce the imaging

force to a minimum and re-adjust the feedback gains until the contrast of the AFM topography is maximal and the error force is minimal (see Step 24). To determine the minimal force, reduce the imaging force to a value at which the stylus does not come into contact with the sample surface anymore. After this goal is achieved, slightly increase the imaging force until the topography of the sample appears. As a control, AFM topographs recorded in the trace and retrace scanning directions should show the same information (e.g., no lateral shift, height difference or structural difference of the biological object). Typical imaging forces are around or below 100 pN.

▲ **CRITICAL STEP** Some AFM systems make it possible to record FD curves at one or a few preset frequencies. Keep in mind that moving the cantilever up and down at small amplitudes comes along with a relatively long contact time between the stylus and the sample. Conversely, larger cantilever amplitudes reduce the contact time and increase the overall velocity of the cantilever. Increasing the contact time increases the probability that the sample nonspecifically adheres to the stylus. As a result, the withdrawing stylus may extract proteins from the membrane or fibril<sup>21,57,97</sup>. Furthermore, when moving the AFM stylus up and down in a sinusoidal manner, the velocity of the AFM stylus is nonlinear. Be aware that the velocity of the AFM stylus (i.e., force-loading rate) affects the mechanical response (e.g., stiffness) of the biological sample<sup>103</sup>. Thus, it is important to define the velocity of the AFM stylus to accurately describe the mechanical properties of a sample.

#### ? TROUBLESHOOTING

**29** | Optimize the feedback gains by increasing the gains in small increments until the system oscillates, which is observed as fringes in the AFM topography or deflection error signal. Then reduce the gains slightly below this value. The scanning line frequency/velocity can be lowered to improve the feedback, as more FD curves per pixel can be achieved; however, recording too many FD curves per scanning area can damage the sample (see Steps 25 and 28).

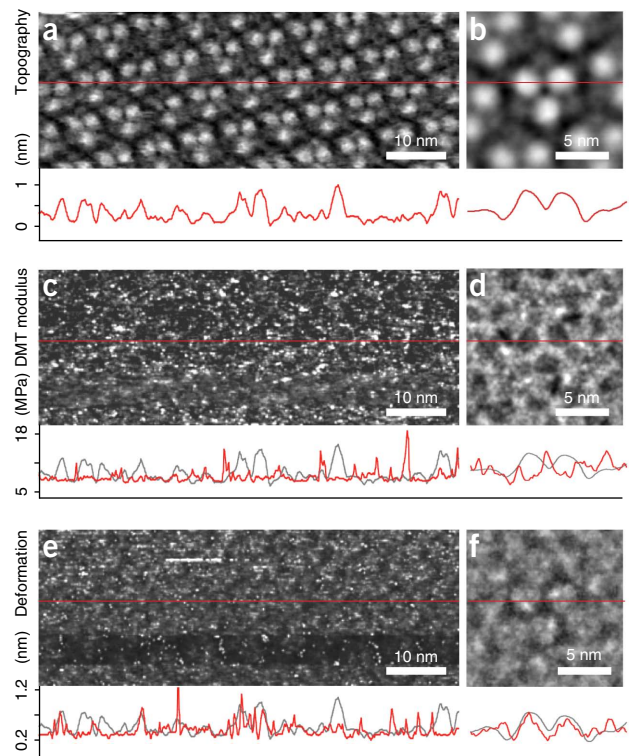
#### ? TROUBLESHOOTING

**30** | Fine-tune the feedback gains until topographic contrast becomes maximal and the imaging force error becomes minimal. The entire process we describe (Steps 28 and 29) may be fine-tuned iteratively.

#### ? TROUBLESHOOTING

**31** | Reoptimize the FD-based AFM parameters when changing the scanning area, scanning speed or any other scanning parameter. Please note that when the scanning speed is too high, the cantilever cannot track the sample properly. As a result, long shadows and streaks will be observed in the topography and imaging force error image.

#### ? TROUBLESHOOTING



## PROTOCOL

**32** | Each time, before zooming into an area of interest (e.g., increasing the magnification by increasing the number of lines scanned per unit area), set the imaging force and feedback gains to an optimum (Steps 28–30). Please note that as magnification increases the FD amplitude may be reduced.

### ? TROUBLESHOOTING

**33** | After zooming into an area of interest, check whether the structural details (e.g., resolution) increase with the number of lines scanned per area. If the structural details increase, the AFM stylus may be sharp. If detail does not improve, the resolution limit is reached. This limit is defined by the sample, stylus and imaging parameters (e.g., scanning line frequency and velocity, frequency and velocity at which the AFM stylus is moved to record FD curves, imaging force and feedback loop).

▲ **CRITICAL STEP** The term (point) resolution refers to the minimum separation of two adjacent points (i.e., pixels) that can be detected and interpreted. The pixel size of the AFM image corresponds to the image size in nanometers divided through the number of lines scanned. Thus, to be able to attain a final lateral resolution of  $\sim 1$  nm, the pixel size needs to be  $\sim 0.5 \times 0.5$  nm<sup>2</sup> or smaller<sup>154,155</sup>.

▲ **CRITICAL STEP** In many cases, the AFM stylus becomes sharper as scanning proceeds. Although very blunt styluses in most cases do not get sufficiently sharp to contour fine structural details, sharp styluses often get sharper over time, allowing high-resolution topographs to be recorded. These stylus changes can be observed by imaging structurally well-defined biological specimen (proteins, in this case). As the stylus shape changes during continuous scanning, the structural details imaged change until finally proteins can be imaged in their native states without an apparent asymmetry or other topographical features being induced by stylus artifacts<sup>156</sup>. In this protocol, imaging a known biological structure such as purple membrane or tau fibrils enables readers to become familiar with the process of optimizing the FD-based AFM imaging parameters and artifacts. In any case, achieving high-resolution FD-based AFM topographs and images takes patience. The operator needs to wait for the stylus to get sufficiently sharp to contour structural details of the proteins. During this time, the operator has to continuously control and optimize the imaging parameters and has to explore whether higher resolution can be achieved on different sample areas on the support.

### ? TROUBLESHOOTING

#### FD curve analysis ● TIMING > 2 h

**34** | Different AFM systems may use different procedures to extract the mechanical parameters recorded by FD-based AFM imaging. The most common parameters that can be extracted from approach and retraction FD curves are deformation, elastic modulus, adhesion and energy dissipation (Fig. 1; see ‘Critical FD curve analysis’). Experimenters should go ahead and extract these parameters. We also recommend that experimenters consult an excellent review on the analysis of FD curves<sup>76</sup>, which will facilitate the thoughtful setting of these parameters. A number of different data analysis options can be implemented, depending on the equipment used. Also in this case, make sure to extract and analyze data by using the capability of your system to its fullest extent. Most FD-based AFM systems (e.g., Bruker, JPK Instruments) come with the option to simultaneously display parametric maps extracted from FD curves while recording the AFM topography.

The recorded FD-based AFM topography can also be saved as an array of FD curves. The analysis software that comes with the AFM systems enables you to extract the FD curves and to analyze them according to user preference (e.g., fit-regions for the contact regime, selection of the model used to calculate the elastic modulus). Furthermore, single FD curves can be selected from the AFM topography and then displayed and analyzed to, for example, extract adhesion forces or deformation values. The FD curves may also be extracted and saved as text or ASCII files for further analysis by user-adaptable software (e.g., MATLAB or Origin).

▲ **CRITICAL STEP** To allow quantitative and comparative measurements of the biological sample, it is important to keep the experimental parameters (e.g., buffer solution, temperature, imaging force, velocity, vertical cantilever amplitude, feedback loop, cantilever) constant and the analysis procedures unchanged.

**35** | (Optional) As already extensively discussed, particularly when working with soft biological specimens, it is required to apply low imaging forces ( $\leq 100$  pN) to prevent irreversible deformation of the specimen. The use of very low imaging forces, however, can have the disadvantage that the FD curves obtained are too noisy to be correctly analyzed. If this is the case, apply higher imaging forces, which may increase the signal-to-noise ratio of the FD curve, and repeat Steps 30 and 31.

▲ **CRITICAL STEP** The imaging force can only be enhanced within certain limits that ensure the integrity of the fragile sample (Step 28).

**36** | (Optional) If the cantilever is too stiff, the mechanical properties of the soft biological sample may not be detected properly (Fig. 4d and ‘Critical cantilever selection’). If this is the case, replace the cantilever with one that has a low spring constant and high deflection sensitivity, as it will greatly improve the acquisition of the mechanical properties. At this point, repeat all steps beginning from Step 17 with the new cantilever.

### ? TROUBLESHOOTING

## ? TROUBLESHOOTING

### Steps 15 and 24

**Problem.** AFM topographs show no protein sample.

**Possible reason.** No proteins may have been adsorbed or AFM imaging parameters must be re-adjusted.

**Solution.** Increase the cantilever amplitude, reduce the imaging force and improve feedback to make sure that protein membranes or fibrils are not brushed off the mica by the scanning AFM stylus. If this approach proves unsuccessful, prepare a new sample by using a different adsorption buffer (one with a higher ionic strength and/or a different pH), a higher protein concentration and a longer adsorption time (Steps 12–16). If the mica is not clean, it may be contaminated by small particles that are present in the protein sample; in this case, make sure to dialyze or to wash your protein sample (see Reagent Setup and Steps 12–16).

### Steps 18, 20 and 22

**Problem.** Periodic or aperiodic deviations of FD curves not related to sample topography.

**Possible reason.** The setup is not in thermal equilibrium or the buffer solution evaporates extensively.

**Solution.** As a permanent solution to this problem, we recommend a temperature-control system that hosts the entire AFM setup, buffer solutions and pipettes, and holds the temperature stable. Alternatively, make sure that the temperature in the environment or room in which the setup is hosted is well controlled, and allow the setup to equilibrate longer before beginning experiments. It may be beneficial to switch on the equipment several hours before the experiment is anticipated to start. Store all buffer solutions and materials used for the experiment in the temperature-controlled environment for several hours before the experiment.

### Steps 20 and 22

**Problem.** When recording approach-retraction FD curves to calibrate the cantilever deflection sensitivity, the deflection signal is irregular and shows irreproducible strong adhesion peaks.

**Possible reason.** The cantilever or sample support is contaminated.

**Solution.** Scan fast over large areas of the support, purple membranes or tau fibrils to brush off contamination. If this approach does not help, mount a new or cleaned cantilever (as in Steps 17 and 18) and/or prepare a new (cleaner) sample (Steps 10–16). If this approach does not help either, make sure that the support, the sample and the buffer solution are clean.

### Step 23

**Problem.** Horizontal and/or vertical offset voltage values of the photodiode change drastically when engaging the AFM stylus.

**Possible reason.** (i) The cantilever is not mounted correctly or AFM is not thermally equilibrated. (ii) The sample support oscillates and may be badly glued or cleaved.

**Solution.** Remount the cantilever (as in Steps 17 and 18) and/or prepare a new sample support (Steps 11–13), and then thermally equilibrate the AFM.

### Step 24

**Problem.** AFM topographs recorded at low resolution are noisy.

**Possible reasons.** (i) AFM feedback gains and/or scanning speed are too high. (ii) Mechanical, thermal or electrical noise interferes with the AFM system.

**Solution.** (i) Adjust feedback gains and scanning speed (Step 24). (ii) Check all mechanical, thermal and electrical noise sources (Steps 5–8).

### Step 24

**Problem.** AFM topographs recorded at low resolution show contamination.

**Possible reason.** The AFM stylus or the sample may be contaminated.

**Solution.** Scan the mica repeatedly at high speed (~20 lines per second), and adjust the frequency by moving the cantilever up and down in order to adjust the scanning line frequency and/or to modulate the forces applied to the AFM cantilever (~100–500 pN) to brush off the contamination from the stylus (Step 24). If the AFM stylus has been cleaned, FD curves recorded on mica show a sharp deflection upon contact of the support (**Fig. 3a,b**; Step 22). The absence of a sharp deflection indicates that either the AFM stylus or mica is contaminated (**Fig. 3c**). If brushing off contaminants was unsuccessful, replace the cantilever (as in Steps 17 and 18) and/or prepare a new (cleaner) sample (Steps 11–18). To prevent contamination of the AFM stylus, it may be helpful to add glycerol (up to 30% (vol/vol)) to the buffer solution. Please note that the stylus-contaminating behavior can vary widely depending on the wafer from which the AFM cantilever was taken. Selecting AFM cantilevers from a different wafer may thus solve the problem.

## PROTOCOL

### Step 24

**Problem.** A large hysteresis is observed between the trace and retrace scanning directions when recording large overview scans ( $>10 \times 10 \mu\text{m}^2$ ).

**Possible reason.** The cantilever is not mounted correctly or the support is prone to oscillations.

**Solution.** Repeat Steps 11–14 (replace the support) and Steps 15 and 16 (adsorb a new sample) or Steps 17–21 (remount and calibrate the cantilever).

### Steps 24 and 27

**Problem.** Simultaneously recorded trace and retrace topography do not overlap.

**Possible reason.** The AFM imaging parameters are not adjusted properly or the sample (or fluid cell) is not tightly fastened to the piezoelectric scanner.

**Solution.** Adjust the imaging force (higher), scanning speed (slower) and feedback gain (higher) (Steps 24–31). If these adjustments do not address the problem, check whether the sample support (or, depending on the AFM used, the fluid cell) is tightly mounted to the piezoelectric scanner.

### Steps 27–33

**Problem.** High-resolution images are unstable and streaky.

**Possible reason.** AFM feedback parameters or/and imaging force are not adjusted properly.

**Solution.** (i) Thermally equilibrate the AFM (Steps 5–8) and optimize the AFM feedback parameters so that the force error channel is minimized (Steps 23–32). (ii) Reduce the force applied to the AFM cantilever. To test whether the applied force was too high, visualize the possible damage. To achieve this, scan a fresh sample area at higher magnification and then scan an overview of the same area at a lower magnification. To reach minimal force, ensure that the drift of the AFM is at its minimum by watching the vertical offset of the cantilever deflection over time.

### Steps 27–33

**Problem.** High-resolution images show artifacts.

**Possible reason.** AFM stylus may be contaminated or shows stylus artifacts: See troubleshooting advice to the problem that can be encountered at Steps 23, 24 and 27–33.

**Solution.** Mount a new/clean AFM cantilever (Steps 17 and 18), calibrate the cantilever (Steps 20–22) and re-image the sample (beginning from Step 24).

### Steps 27–33

**Problem.** High-resolution images are strongly distorted, showing either a large hysteresis between the trace and retrace scanning direction or sample features deformed along different scanning directions.

**Possible reason.** Sample preparation is of insufficient quality or the cantilever is defective.

**Solution.** Check the quality of sample preparation. Is the glue evenly spread under the mica? Is the mica tightly coupled to its support (Steps 1–4)? Is there any dirt or dust lodged between the sample holder and the sample (see Reagent Setup)? Has the fluid cell been mounted correctly (Step 18)? Make sure that the cantilever is not defective and check that the calibration of the piezoelectric scanner is correct (Steps 20–22).

### Steps 27–33

**Problem.** High-resolution images (e.g., topography, force error) show oscillations at minimal force.

**Possible reason.** AFM feedback gains and/or scanning speed are too high.

**Solution.** Optimize the gains and scanning speed. If required, realign the laser to optimize the diode signal. If an expected molecular symmetry (e.g., bacteriorhodopsin trimer or protein fibril) is not observed, change and calibrate the AFM cantilever by implementing Steps 17–22.

### Steps 27–33

**Problem.** In spite of all efforts, the resolution of the AFM topograph remains mediocre.

**Possible reason.** (i) AFM imaging force, feedback gains or speed are not optimized. (ii) The AFM stylus is not sharp enough.

**Solution.** Repeatedly optimize the AFM imaging parameters (Steps 27–32). If the resolution of the AFM topograph does not improve (see Step 33), change and calibrate the AFM cantilever by implementing Steps 17–22.

### ● TIMING

To become familiar handling the sample, support and AFM, it takes an AFM beginner at least 2–4 weeks of training, after that the following timings can be used as guidance.

Steps 1–4, day 1, preparation of mounting supports: 2–8 h  
 Steps 5–8, day 1, setting up the AFM: 1–8 h  
 Steps 9 and 10, day 2, choosing the AFM cantilever and cleaning the AFM components: ~1 h  
 Steps 11–19, day 2, adsorption of membranes or tau fibrils: ~1 h  
 Steps 20–22, day 2, calibration and checking for contamination of the cantilever: 10 min  
 Steps 23–26, day 2, low-resolution FD-based AFM imaging: ~1 h  
 Steps 27–33, subsequent days, high-resolution AFM imaging: 2–4 h (after 2–4 weeks of training)  
 Steps 34–36, FD curve analysis: >2 h (depending on the degree of post-treatment of the FD curves, e.g., with MATLAB)

## ANTICIPATED RESULTS

Depending on the sample corrugation, native membrane proteins are expected to be imaged at ~1-nm resolution. Flat membranes, such as purple membranes, which show 2D bacteriorhodopsin assemblies with protrusions less than 1 nm in height, will allow sub-nanometer resolution and thus the visualization of polypeptide loops that connect individual transmembrane  $\alpha$ -helices. Depending on the imaging force applied, FD-based AFM enables the imaging of the polypeptide loops in the unperturbed state. Proteins and fibrils that protrude by more than 3 nm from the mica surface may be imaged at a resolution approaching 2 nm, because such 'large' protrusions are likely to be structurally flexible and their protruding height prevents the proper contouring of the sample surface by the AFM stylus. Consequently, examples shown in **Figures 2, 4 and 5** can be obtained routinely by using the software provided with the AFM systems mentioned in the MATERIALS section.

The acquisition of FD curves from single membrane-embedded proteins is easy, although the correct analysis and full interpretation of the FD curves requires expertise and may become challenging. As the cleanliness and stability of the instrument are major requisites for obtaining high-resolution FD-AFM data of the biological specimen, relevant precautions must be taken to prevent contamination, as contaminants may introduce artifacts in recording FD curves at molecular resolution.

**ACKNOWLEDGMENTS** We thank D. Alsteens and I. Medalsy for stimulating discussions and advice. This work was supported by the Swiss National Science Foundation, the European Union Marie Curie Actions program through the ACRITAS Initial Training Network (FP7-PEOPLE-2012-ITN, Project 317348), and the European Molecular Biology Organization long-term fellowship 506-2012.

**AUTHOR CONTRIBUTIONS** M.P., D.M.-M., S.W. and D.J.M. designed the AFM protocol. M.P., E.M. and S.W. performed and optimized the experimental procedure. M.P., D.M.-M., S.W. and D.J.M. wrote the manuscript.

**COMPETING FINANCIAL INTERESTS** The authors declare no competing financial interests.

Reprints and permissions information is available online at <http://www.nature.com/reprints/index.html>.

1. Roux, B. & MacKinnon, R. The cavity and pore helices in the KcsA  $K^+$  channel: electrostatic stabilization of monovalent cations. *Science* **285**, 100–102 (1999).
2. Karplus, M. & Gao, Y.Q. Biomolecular motors: the  $F_1$ -ATPase paradigm. *Curr. Opin. Struct. Biol.* **14**, 250–259 (2004).
3. Sotomayor, M. & Schulten, K. Single-molecule experiments *in vitro* and *in silico*. *Science* **316**, 1144–1148 (2007).
4. Whorton, M.R. & MacKinnon, R. X-ray structure of the mammalian GIRK2- $\beta$  G-protein complex. *Nature* **498**, 190–197 (2013).
5. Stansfeld, P.J. & Sansom, M.S. Molecular simulation approaches to membrane proteins. *Structure* **19**, 1562–1572 (2011).
6. Risselada, H.J. & Grubmuller, H. How SNARE molecules mediate membrane fusion: recent insights from molecular simulations. *Curr. Opin. Struct. Biol.* **22**, 187–196 (2012).
7. Dufrene, Y.F. *et al.* Five challenges to bringing single-molecule force spectroscopy into living cells. *Nat. Methods* **8**, 123–127 (2011).
8. Veigel, C. & Schmidt, C.F. Moving into the cell: single-molecule studies of molecular motors in complex environments. *Nat. Rev. Mol. Cell Biol.* **12**, 163–176 (2011).
9. Ha, T. Single-molecule approaches embrace molecular cohorts. *Cell* **154**, 723–726 (2013).
10. Larson, J.D., Rodgers, M.L. & Hoskins, A.A. Visualizing cellular machines with colocalization single molecule microscopy. *Chem. Soc. Rev.* **43**, 1189–1200 (2013).
11. Heinz, W.F. & Hoh, J.H. Spatially resolved force spectroscopy of biological surfaces using the atomic force microscope. *Trends Biotechnol.* **17**, 143–150 (1999).
12. Dufrene, Y.F., Martinez-Martin, D., Medalsy, I., Alsteens, D. & Muller, D.J. Multiparametric imaging of biological systems by force-distance curve-based AFM. *Nat. Methods* **10**, 847–854 (2013).
13. Binnig, G., Quate, C.F. & Gerber, C. Atomic force microscope. *Phys. Rev. Lett.* **56**, 930–933 (1986).
14. Gerber, C. & Lang, H.P. How the doors to the nanoworld were opened. *Nat. Nanotechnol.* **1**, 3–5 (2006).
15. Muller, D.J. & Dufrene, Y.F. Atomic force microscopy as a multifunctional molecular toolbox in nanobiotechnology. *Nat. Nanotechnol.* **3**, 261–269 (2008).
16. Drake, B. *et al.* Imaging crystals, polymers, and processes in water with the atomic force microscope. *Science* **243**, 1586–1589 (1989).
17. Karrasch, S., Hegerl, R., Hoh, J., Baumeister, W. & Engel, A. Atomic force microscopy produces faithful high-resolution images of protein surfaces in an aqueous environment. *Proc. Natl. Acad. Sci. USA* **91**, 836–838 (1994).
18. Schabert, F.A., Henn, C. & Engel, A. Native *Escherichia coli* OmpF porin surfaces probed by atomic force microscopy. *Science* **268**, 92–94 (1995).
19. Mou, J., Yang, J. & Shao, Z. Atomic force microscopy of cholera toxin B-oligomers bound to bilayers of biologically relevant lipids. *J. Mol. Biol.* **248**, 507–512 (1995).
20. Müller, D.J., Schabert, F.A., Büldt, G. & Engel, A. Imaging purple membranes in aqueous solutions at sub-nanometer resolution by atomic force microscopy. *Biophys. J.* **68**, 1681–1686 (1995).
21. Müller, D.J. & Engel, A. Atomic force microscopy and spectroscopy of native membrane proteins. *Nat. Protoc.* **2**, 2191–2197 (2007).
22. Heymann, J.B. *et al.* Charting the surfaces of the purple membrane. *J. Struct. Biol.* **128**, 243–249 (1999).
23. Müller, D.J., Sass, H.J., Müller, S.A., Büldt, G. & Engel, A. Surface structures of native bacteriorhodopsin depend on the molecular packing arrangement in the membrane. *J. Mol. Biol.* **285**, 1903–1909 (1999).

## PROTOCOL

24. Müller, D.J. & Engel, A. Voltage and pH-induced channel closure of porin OmpF visualized by atomic force microscopy. *J. Mol. Biol.* **285**, 1347–1351 (1999).
25. Engel, A. & Müller, D.J. Observing single biomolecules at work with the atomic force microscope. *Nat. Struct. Biol.* **7**, 715–718 (2000).
26. Bippes, C.A. & Müller, D.J. High-resolution atomic force microscopy and spectroscopy of native membrane proteins. *Rep. Progr. Phys.* **74**, 086601 (2011).
27. Müller, D.J., Baumeister, W. & Engel, A. Conformational change of the hexagonally packed intermediate layer of *Deinococcus radiodurans* imaged by atomic force microscopy. *J. Bacteriol.* **178**, 3025–3030 (1996).
28. Mari, S.A. *et al.* pH-induced conformational change of the  $\beta$ -barrel-forming protein OmpG reconstituted into native *E. coli* lipids. *J. Mol. Biol.* **396**, 610–616 (2010).
29. Müller, D.J., Hand, G.M., Engel, A. & Sosinsky, G. Conformational changes in surface structures of isolated Connexin26 gap junctions. *EMBO J.* **21**, 3598–3607 (2002).
30. Yu, J., Bippes, C.A., Hand, G.M., Müller, D.J. & Sosinsky, G.E. Aminosulfonate modulated pH-induced conformational changes in connexin26 hemichannels. *J. Biol. Chem.* **282**, 8895–8904 (2007).
31. Shibata, M., Uchihashi, T., Yamashita, H., Kandori, H. & Ando, T. Structural changes in bacteriorhodopsin in response to alternate illumination observed by high-speed atomic force microscopy. *Angew. Chem. Int. Ed. Engl.* **50**, 4410–4413 (2011).
32. Shibata, M., Yamashita, H., Uchihashi, T., Kandori, H. & Ando, T. High-speed atomic force microscopy shows dynamic molecular processes in photoactivated bacteriorhodopsin. *Nat. Nanotechnol.* **5**, 208–212 (2010).
33. Shinozaki, Y. *et al.* Direct observation of ATP-induced conformational changes in single P2X<sub>4</sub> receptors. *PLoS Biol.* **7**, e1000103 (2009).
34. Mari, S.A. *et al.* Gating of the MloT1 potassium channel involves large rearrangements of the cyclic nucleotide-binding domains. *Proc. Natl. Acad. Sci. USA* **108**, 20802–20807 (2011).
35. Sumino, A., Sumikama, T., Iwamoto, M., Dewa, T. & Oiki, S. The open gate structure of the membrane-embedded KcsA potassium channel viewed from the cytoplasmic side. *Sci. Rep.* **3**, 1063 (2013).
36. Fotiadis, D. *et al.* Surface analysis of the photosystem I complex by electron and atomic force microscopy. *J. Mol. Biol.* **283**, 83–94 (1998).
37. Revakine, I., Bergsma-Schutter, W. & Brisson, A. Growth of protein 2D crystals on supported planar lipid bilayers imaged *in situ* by AFM. *J. Struct. Biol.* **121**, 356–361 (1998).
38. Seelert, H. *et al.* Proton powered turbine of a plant motor. *Nature* **405**, 418–419 (2000).
39. Müller, D.J. *et al.* ATP synthase: constrained stoichiometry of the transmembrane rotor. *FEBS Lett.* **504**, 219–222 (2001).
40. Müller, D.J. *et al.* Observing membrane protein diffusion at subnanometer resolution. *J. Mol. Biol.* **327**, 925–930 (2003).
41. Czajkowsky, D.M., Hotze, E.M., Shao, Z. & Tweten, R.K. Vertical collapse of a cytolysin prepore moves its transmembrane  $\beta$ -hairpins to the membrane. *EMBO J.* **23**, 3206–3215 (2004).
42. Yamashita, H. *et al.* Single-molecule imaging on living bacterial cell surface by high-speed AFM. *J. Mol. Biol.* **422**, 300–309 (2012).
43. Zhong, Q., Inniss, D., Kjoller, K. & Elings, V. Fractured polymer silica fiber surface studied by tapping mode atomic-force microscopy. *Surf. Sci.* **290**, L688–L692 (1993).
44. Hansma, P.K. *et al.* Tapping mode atomic-force microscopy in liquids. *Appl. Phys. Lett.* **64**, 1738–1740 (1994).
45. Putman, C.A.J., Vanderwerf, K.O., Degrooth, B.G., Vanhulst, N.F. & Greve, J. Tapping mode atomic-force microscopy in liquid. *Appl. Phys. Lett.* **64**, 2454–2456 (1994).
46. Bezanilla, M. *et al.* Motion and enzymatic degradation of DNA in the atomic force microscope. *Biophys. J.* **67**, 2454–2459 (1994).
47. Radmacher, M., Fritz, M., Hansma, H.G. & Hansma, P.K. Direct observation of enzyme activity with the atomic force microscope. *Science* **265**, 1577–1579 (1994).
48. Fritz, M. *et al.* Imaging microtubules in buffer solution using tapping mode atomic force microscopy. *SPIE* **2384**, 150–157 (1995).
49. Martin, L.D., Vesenka, J.P., Henderson, E. & Dobbs, D.L. Visualization of nucleosomal substructure in native chromatin by atomic force microscopy. *Biochem.* **34**, 4610–4616 (1995).
50. Dunlap, D.D., Maggi, A., Soria, M.R. & Monaco, L. Nanoscopic structure of DNA condensed for gene delivery. *Nucl. Acids Res.* **25**, 3095–3101 (1997).
51. Kasas, S. *et al.* *Escherichia coli* RNA polymerase activity observed using atomic force microscopy. *Biochemistry* **36**, 461–468 (1997).
52. Lyubchenko, Y.L. & Shlyakhtenko, L.S. Direct visualization of supercoiled DNA *in situ* with atomic force microscopy. *Proc. Natl. Acad. Sci. USA* **94**, 496–501 (1997).
53. Franz, C.M. & Müller, D.J. Analysing focal adhesion structure by AFM. *J. Cell Sci.* **118**, 5315–5323 (2005).
54. Elie-Caille, C. *et al.* Straight GDP-tubulin protofilaments form in the presence of taxol. *Curr. Biol.* **17**, 1765–1770 (2007).
55. Erler, A. *et al.* Conformational adaptability of Red $\beta$  during DNA annealing and implications for its structural relationship with Rad52. *J. Mol. Biol.* **391**, 586–598 (2009).
56. Koderer, N., Yamamoto, D., Ishikawa, R. & Ando, T. Video imaging of walking myosin V by high-speed atomic force microscopy. *Nature* **468**, 72–76 (2010).
57. Wegmann, S. *et al.* Human tau isoforms assemble into ribbon-like fibrils that display polymorphic structure and stability. *J. Biol. Chem.* **285**, 27302–27313 (2010).
58. Möller, C., Allen, M., Elings, V., Engel, A. & Müller, D.J. Tapping mode atomic force microscopy produces faithful high-resolution images of protein surfaces. *Biophys. J.* **77**, 1050–1058 (1999).
59. Stark, M., Möller, C., Müller, D.J. & Guckenberger, R. From images to interactions: high-resolution phase imaging in tapping-mode atomic force microscopy. *Biophys. J.* **80**, 3009–3018 (2001).
60. Garcia, R. & Perez, R. Dynamic atomic force microscopy methods. *Surf. Sci. Rep.* **47**, 197–301 (2002).
61. Stark, M., Stark, R.W., Heckl, W.M. & Guckenberger, R. Inverting dynamic force microscopy: from signals to time-resolved interaction forces. *Proc. Natl. Acad. Sci. USA* **99**, 8473–8478 (2002).
62. Basak, S. & Raman, A. Dynamics of tapping mode atomic force microscopy in liquids: theory and experiments. *Appl. Phys. Lett.* **91**, 064107 (2007).
63. Garcia, R. & Herruzo, E.T. The emergence of multifrequency force microscopy. *Nat. Nanotechnol.* **7**, 217–226 (2012).
64. Argaman, M., Golan, R., Thomson, N.H. & Hansma, H.G. Phase imaging of moving DNA molecules and DNA molecules replicated in the atomic force microscope. *Nucleic Acids Res.* **25**, 4379–4383 (1997).
65. Viani, M.B. *et al.* Probing protein-protein interactions in real time. *Nat. Struct. Biol.* **7**, 644–647 (2000).
66. Uchihashi, T., Iino, R., Ando, T. & Noji, H. High-speed atomic force microscopy reveals rotary catalysis of rotorless F<sub>1</sub>-ATPase. *Science* **333**, 755–758 (2011).
67. Hoh, J.H., Lal, R., John, S.A., Revel, J.-P. & Arnsdorf, M.F. Atomic force microscopy and dissection of gap junctions. *Science* **253**, 1405–1408 (1991).
68. Hansma, H.G. *et al.* Reproducible imaging and dissection of plasmid DNA under liquid with the atomic force microscope. *Science* **256**, 1180–1184 (1992).
69. Thalhammer, S., Stark, R.W., Müller, S., Wienberg, J. & Heckl, W.M. The atomic force microscope as a new microdissecting tool for the generation of genetic probes. *J. Struct. Biol.* **119**, 232–237 (1997).
70. Weisenhorn, A.L., Hansma, P.K., Albrecht, T.R. & Quate, C.F. Forces in atomic force microscopy in air and water. *Appl. Phys. Lett.* **54**, 2651–2653 (1989).
71. Butt, H.J. Measuring electrostatic, van der Waals, and hydration forces in electrolyte solutions with an atomic force microscope. *Biophys. J.* **60**, 1438–1444 (1991).
72. Ducker, W.A., Senden, T.J. & Pashley, R.M. Direct measurement of colloidal forces using an atomic force microscope. *Nature* **353**, 239–241 (1991).
73. Butt, H.J. Electrostatic interaction in scanning probe microscopy when imaging in electrolyte solutions. *Nanotechnology* **3**, 60–68 (1992).
74. Weisenhorn, A.L., Maivald, P., Butt, H.J. & Hansma, P.K. Measuring adhesion, attraction, and repulsion between surfaces in liquids with an atomic-force microscope. *Phys. Rev. B* **45**, 11226–11232 (1992).
75. Knapp, H.F., Wiegbräde, W., Heim, M., Eschrich, R. & Guckenberger, R. Atomic force microscope measurements and manipulation of Langmuir-Blodgett films with modified tips. *Biophys. J.* **69**, 708–715 (1995).
76. Butt, H.J., Cappella, B. & Kappl, M. Force measurements with the atomic force microscope: technique, interpretation and applications. *Surf. Sci. Rep.* **59**, 1–152 (2005).
77. Lee, G.U., Kidwell, D.A. & Colton, R.J. Sensing discrete streptavidin-biotin interactions with atomic force microscopy. *Langmuir* **10**, 354–357 (1994).
78. Florin, E.-L., Moy, V.T. & Gaub, H.E. Adhesion forces between individual ligand-receptor pairs. *Science* **264**, 415–417 (1994).
79. Moy, V.T., Florin, E.-L. & Gaub, H.E. Intermolecular forces and energies between ligands and receptors. *Science* **266**, 257–259 (1994).
80. Radmacher, M., Cleveland, J.P., Fritz, M., Hansma, H.G. & Hansma, P.K. Mapping interaction forces with the atomic force microscope. *Biophys. J.* **66**, 2159–2165 (1994).
81. Ludwig, M., Dettmann, W. & Gaub, H.E. Atomic force microscope imaging contrast based on molecular recognition. *Biophys. J.* **72**, 445–448 (1997).
82. Gad, M., Itoh, A. & Ikai, A. Mapping cell wall polysaccharides of living microbial cells using atomic force microscopy. *Cell Biol. Int.* **21**, 697–706 (1997).

83. Grandbois, M., Dettmann, W., Benoit, M. & Gaub, H.E. Affinity imaging of red blood cells using an atomic force microscope. *J. Histochem. Cytochem.* **48**, 719–724 (2000).

84. Hinterdorfer, P. & Dufrene, Y.F. Detection and localization of single molecular recognition events using atomic force microscopy. *Nat. Methods* **3**, 347–355 (2006).

85. Roos, W.H., Bruinsma, R. & Wuite, G.J.L. Physical virology. *Nat. Phys.* **6**, 733–743 (2010).

86. Alsteens, D., Trabelsi, H., Soumillion, P. & Dufrene, Y.F. Multiparametric atomic force microscopy imaging of single bacteriophages extruding from living bacteria. *Nat. Commun.* **4**, 2926 (2013).

87. Medalsy, I., Hensen, U. & Muller, D.J. Imaging and quantifying chemical and physical properties of native proteins at molecular resolution by force-volume AFM. *Angew. Chem. Int. Ed. Engl.* **50**, 12103–12108 (2011).

88. Thoma, J., Bosshart, P., Pfreundschuh, M. & Muller, D.J. Out but not in: the large transmembrane  $\beta$ -barrel protein FhuA unfolds but cannot refold via  $\beta$ -hairpins. *Structure* **20**, 2185–2190 (2012).

89. Pfreundschuh, M., Hensen, U. & Muller, D.J. Quantitative imaging of the electrostatic field and potential generated by a single transmembrane protein at subnanometer resolution. *Nano Lett.* **13**, 5585–5593 (2013).

90. Sweers, K.K., van der Werf, K.O., Bennink, M.L. & Subramaniam, V. Atomic force microscopy under controlled conditions reveals structure of C-terminal region of  $\alpha$ -synuclein in amyloid fibrils. *ACS Nano* **6**, 5952–5960 (2012).

91. Zhang, S. *et al.* Coexistence of ribbon and helical fibrils originating from hIAPP<sub>20–29</sub> revealed by quantitative nanomechanical atomic force microscopy. *Proc. Natl. Acad. Sci. USA* **110**, 2798–2803 (2013).

92. Wegmann, S., Medalsy, I.D., Mandelkow, E. & Muller, D.J. The fuzzy coat of pathological human tau fibrils is a two-layered polyelectrolyte brush. *Proc. Natl. Acad. Sci. USA* **110**, E313–E321 (2013).

93. Muller, D.J., Buldt, G. & Engel, A. Force-induced conformational change of bacteriorhodopsin. *J. Mol. Biol.* **249**, 239–243 (1995).

94. Butt, H.-J., Prater, C.B. & Hansma, P.K. Imaging purple membranes dry and in water with the atomic force microscope. *J. Vac. Sci. Technol.* **B9**, 1193–1197 (1991).

95. Butt, H.J. Measuring local surface charge densities in electrolyte solutions with a scanning-force microscope. *Biophys. J.* **63**, 578–582 (1992).

96. Muller, D.J. *et al.* Atomic force microscopy of native purple membrane. *Biochim. Biophys. Acta* **1460**, 27–38 (2000).

97. Oesterhelt, F. *et al.* Unfolding pathways of individual bacteriorhodopsins. *Science* **288**, 143–146 (2000).

98. Muller, D.J. *et al.* Stability of bacteriorhodopsin  $\alpha$ -helices and loops analyzed by single-molecule force spectroscopy. *Biophys. J.* **83**, 3578–3588 (2002).

99. Janovjak, H., Kessler, M., Oesterhelt, D., Gaub, H. & Muller, D.J. Unfolding pathways of native bacteriorhodopsin depend on temperature. *EMBO J.* **22**, 5220–5229 (2003).

100. Kienberger, F., Kada, G., Mueller, H. & Hinterdorfer, P. Single-molecule studies of antibody-antigen interaction strength versus intramolecular antigen stability. *J. Mol. Biol.* **347**, 597–606 (2005).

101. Kessler, M., Gottschalk, K.E., Janovjak, H., Muller, D.J. & Gaub, H.E. Bacteriorhodopsin folds into the membrane against an external force. *J. Mol. Biol.* **357**, 644–654 (2006).

102. Muller, D.J. *et al.* Single-molecule studies of membrane proteins. *Curr. Opin. Struct. Biol.* **16**, 489–495 (2006).

103. Medalsy, I.D. & Muller, D.J. Nanomechanical properties of proteins and membranes depend on loading rate and electrostatic interactions. *ACS Nano* **7**, 2642–2650 (2013).

104. Goldsbury, C., Kistler, J., Aebi, U., Arvinte, T. & Cooper, G.J. Watching amyloid fibrils grow by time-lapse atomic force microscopy. *J. Mol. Biol.* **285**, 33–39 (1999).

105. Yip, C.M. & McLaurin, J. Amyloid- $\beta$  peptide assembly: a critical step in fibrillogenesis and membrane disruption. *Biophys. J.* **80**, 1359–1371 (2001).

106. Grundke-Iqbali, I. *et al.* Microtubule-associated protein tau. A component of Alzheimer paired helical filaments. *J. Biol. Chem.* **261**, 6084–6089 (1986).

107. Mandelkow, E.M. & Mandelkow, E. Biochemistry and cell biology of tau protein in neurofibrillary degeneration. *Cold Spring Harb. Perspect. Med.* **2**, a006247 (2012).

108. Tanaka, M. & Sackmann, E. Polymer-supported membranes as models of the cell surface. *Nature* **437**, 656–663 (2005).

109. Muller, D.J. & Engel, A. Strategies to prepare and characterize native membrane proteins and protein membranes by AFM. *Curr. Opin. Coll. Int. Sci.* **13**, 338–350 (2008).

110. Muller, D.J., Amrein, M. & Engel, A. Adsorption of biological molecules to a solid support for scanning probe microscopy. *J. Struct. Biol.* **119**, 172–188 (1997).

111. Fotiadis, D., Scheuring, S., Muller, S.A., Engel, A. & Muller, D.J. Imaging and manipulation of biological structures with the AFM. *Microsc. Microanal.* **33**, 385–397 (2002).

112. Pashley, R.M. Hydration forces between mica surfaces in aqueous electrolyte solutions. *J. Coll. Interf. Sci.* **80**, 153–162 (1981).

113. Bailey, S.W. (Ed.) *Micas. Rev. Mineral.* **13** (1984).

114. Gerischer, H., McIntyre, R., Scherson, D. & Storck, W. Density of the electronic states of graphite: derivation from differential capacitance measurements. *J. Phys. Chem.* **91**, 1930–1935 (1987).

115. Martínez-Martín, D. *et al.* Atmospheric contaminants on graphitic surfaces. *Carbon* **61**, 33–39 (2013).

116. Neuman, K.C. & Nagy, A. Single-molecule force spectroscopy: optical tweezers, magnetic tweezers and atomic force microscopy. *Nat. Methods* **5**, 491–505 (2008).

117. Muller, D.J., Helenius, J., Alsteens, D. & Dufrene, Y.F. Force-probing surfaces of living cells to molecular resolution. *Nat. Chem. Biol.* **5**, 383–390 (2009).

118. Alcaraz, J. *et al.* Correction of microrheological measurements of soft samples with atomic force microscopy for the hydrodynamic drag on the cantilever. *Langmuir* **18**, 716–721 (2002).

119. Janovjak, H., Struckmeier, J. & Muller, D.J. Hydrodynamic effects in fast AFM single-molecule force measurements. *Eur. Biophys. J.* **34**, 91–96 (2005).

120. Viani, M.B. *et al.* Small cantilevers for force spectroscopy of single molecules. *J. Appl. Phys.* **86**, 2258–2262 (1999).

121. Hansma, P.K., Schitter, G., Fantner, G.E. & Prater, C. Applied physics. High-speed atomic force microscopy. *Science* **314**, 601–602 (2006).

122. Zimmermann, J.L., Nicolaus, T., Neuert, G. & Blank, K. Thiol-based, site-specific and covalent immobilization of biomolecules for single-molecule experiments. *Nat. Protoc.* **5**, 975–985 (2010).

123. Martinez-Martín, D., Herruzo, E.T., Dietz, C., Gomez-Herrero, J. & Garcia, R. Noninvasive protein structural flexibility mapping by bimodal dynamic force microscopy. *Phys. Rev. Lett.* **106**, 198101 (2011).

124. Martinez-Martín, D. *et al.* Resolving structure and mechanical properties at the nanoscale of viruses with frequency modulation atomic force microscopy. *PLoS ONE* **7**, e30204 (2012).

125. Rotsch, C. & Radmacher, M. Mapping local electrostatic forces with the atomic force microscope. *Langmuir* **13**, 2825–2832 (1997).

126. Matzke, R., Jacobson, K. & Radmacher, M. Direct, high-resolution measurement of furrow stiffening during division of adherent cells. *Nat. Cell Biol.* **3**, 607–610 (2001).

127. Heu, C., Berquand, A., Elie-Caille, C. & Nicod, L. Glyphosate-induced stiffening of HaCat keratinocytes, a peak force tapping study on living cells. *J. Struct. Biol.* **178**, 1–7 (2012).

128. Carrasco, C. *et al.* Built-in mechanical stress in viral shells. *Biophys. J.* **100**, 1100–1108 (2011).

129. Dong, M., Husale, S. & Sahin, O. Determination of protein structural flexibility by microsecond force spectroscopy. *Nat. Nanotechnol.* **4**, 514–517 (2009).

130. Picas, L., Rico, F., Deforet, M. & Scheuring, S. Structural and mechanical heterogeneity of the erythrocyte membrane reveals membrane stability. *ACS Nano* **7**, 1054–1063 (2013).

131. Grant, C.A., Brockwell, D.J., Radford, S.E. & Thomson, N.H. Tuning the elastic modulus of hydrated collagen fibrils. *Biophys. J.* **97**, 2985–2992 (2009).

132. Sweers, K., van der Werf, K., Bennink, M. & Subramaniam, V. Nanomechanical properties of alpha-synuclein amyloid fibrils: a comparative study by nanoindentation, harmonic force microscopy, and Peakforce QNM. *Nanoscale Res. Lett.* **6**, 270 (2011).

133. Sullan, R.M., Li, J.K. & Zou, S. Direct correlation of structures and nanomechanical properties of multicomponent lipid bilayers. *Langmuir* **25**, 7471–7477 (2009).

134. Li, J.K., Sullan, R.M. & Zou, S. Atomic force microscopy force mapping in the study of supported lipid bilayers. *Langmuir* **27**, 1308–1313 (2011).

135. Rief, M., Fernandez, J.M. & Gaub, H.E. Elastically coupled two-level-systems as a model for biopolymer extensibility. *Phys. Rev. Lett.* **81**, 4764–4767 (1998).

136. Grandbois, M., Beyer, M., Rief, M., Clausen-Schaumann, H. & Gaub, H.E. How strong is a covalent bond? *Science* **283**, 1727–1730 (1999).

137. Rief, M., Clausen-Schaumann, H. & Gaub, H.E. Sequence-dependent mechanics of single DNA molecules. *Nat. Struct. Biol.* **6**, 346–349 (1999).

138. Higgins, M.J. *et al.* Structured water layers adjacent to biological membranes. *Biophys. J.* **91**, 2532–2542 (2006).

## PROTOCOL

139. Pelling, A.E., Sehati, S., Gralla, E.B., Valentine, J.S. & Gimzewski, J.K. Local nanomechanical motion of the cell wall of *Saccharomyces cerevisiae*. *Science* **305**, 1147–1150 (2004).

140. Baclayon, M., Roos, W.H. & Wuite, G.J. Sampling protein form and function with the atomic force microscope. *Mol. Cell Proteomics* **9**, 1678–1688 (2010).

141. Hertz, H. Über die Berührung fester elastischer Körper. *Reine Angew. Math.* **92**, 156–171 (1881).

142. Johnson, K.L., Kendall, K. & Roberts, A.D. Surface energy and contact of elastic solids. *Proc. R. Soc. A* **324**, 301–313 (1971).

143. Derjaguin, B.V., Muller, V.M. & Toporov, Y.P. Effect of contact deformations on adhesion of particles. *J. Coll. Interf. Sci.* **53**, 314–326 (1975).

144. Muller, V.M., Yushchenko, V.S. & Derjaguin, B.V. On the influence of molecular forces on the deformation of an elastic sphere and its sticking to a rigid plane. *J. Coll. Interf. Sci.* **77**, 91–101 (1980).

145. Muller, V.M., Derjaguin, B.V. & Toporov, Y.P. On 2 methods of calculation of the force of sticking of an elastic sphere to a rigid plane. *Coll. Surf.* **7**, 251–259 (1983).

146. Oesterhelt, D. & Stoeckenius, W. Isolation of the cell membrane of *Halobacterium halobium* and its fraction into red and purple membrane. *Methods Enzymol.* **31**, 667–678 (1974).

147. Barghorn, S., Biernat, J. & Mandelkow, E. Purification of recombinant tau protein and preparation of Alzheimer-paired helical filaments *in vitro*. *Methods Mol. Biol.* **299**, 35–51 (2005).

148. Müller, D.J., Engel, A. & Amrein, M. Preparation techniques for the observation of native biological systems with the atomic force microscope. *Biosens. Bioelect.* **12**, 867–877 (1997).

149. Sader, J.E. & White, L. Theoretical analysis of the static deflection of plates for atomic force microscope applications. *J. Appl. Phys.* **74**, 1–9 (1993).

150. Butt, H.J. & Jaschke, M. Calculation of thermal noise in atomic-force microscopy. *Nanotechnology* **6**, 1–7 (1995).

151. Florin, E.L. *et al.* Sensing specific molecular-interactions with the atomic-force microscope. *Biosensors Bioelectron.* **10**, 895–901 (1995).

152. Hutter, J.L. & Bechhoefer, J. Calibration of atomic-force microscope tips. *Rev. Sci. Instr.* **64**, 1868–1873 (1993).

153. te Riet, J. *et al.* Interlaboratory round robin on cantilever calibration for AFM force spectroscopy. *Ultramicroscopy* **111**, 1659–1669 (2011).

154. Engel, A., Schoenenberger, C.A. & Muller, D.J. High resolution imaging of native biological sample surfaces using scanning probe microscopy. *Curr. Opin. Struct. Biol.* **7**, 279–284 (1997).

155. Heymann, J.B., Moeller, C. & Muller, D.J. Sampling effects influence heights measured with atomic force microscopy. *J. Microsc.* **207**, 43–51 (2001).

156. Schwarz, U.D., Haefke, H., Reimann, P. & Guntherodt, H.J. Tip artefacts in scanning force microscopy. *J. Microsc.* **173**, 183–197 (1994).